on-off switching without PID control in order to examine the capability of supporting natural cardiac contractile function.

Left ventricular (LV) pressure was measured by a catheter tip transducer (Millar, SVPC-664A), and LV volume was obtained by a conductance catheter (Taisho-Ika, Sigma-5). Each sensor was inserted at the left atrial portion through the mitral valve. The data was recorded by a digital recording unit (TEAC, LX-10) and the sampling frequency was 1.5kHz.

3. RESULTS AND DISCUSSION

3.1 PID control for the displacement

As shown in Fig. 5 and 6, the accurate displacement control could be achieved in each shape memory alloy fibre by the PID control under the different tensile forced condition by using different bias spring, as well as the different ambient heat transfer condition, which was obtained from the test circuit as shown in Fig. 2.

3.2 Pressure-volume relationships in a goat

Fig. 4 shows that the external cardiac work was elevated by the mechanical assistance using a myocardial assist device. As a result, it was indicated that the synchronous mechanical assistance by using the system might be effective for the artificial circulatory support for the patients with chronic heart failure or angina of effort.

4. CONCLUSION

Functional changes of the covalent type shape memory alloy fibre were examined. And it was indicated that the capability of the sophisticated functional reproduction of natural myocardial contraction could be represented by using the PID control method.

As the contractile tensile force and shortening of myocardial tissues might be adopted to each hemodynamic condition, it was suggested that these methods for the control of the fibres might be useful to achieve more effective assistance by the artificial myocardium system.

And myocardial assistive device has been developed and it was suggested that the effective assistance could be achieved in goats. When it is attached onto the ventricular wall, it should be considered the forced refrigerant effect by blood circulation such as coronary perfusion during the PID control..

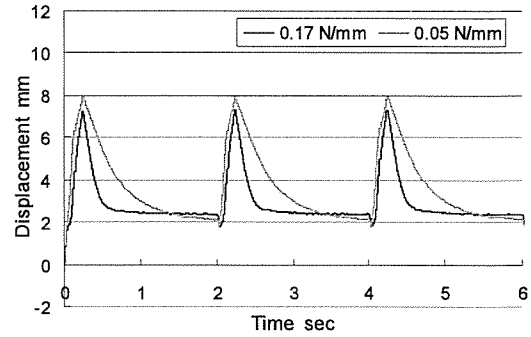

(a) Bias spring effect – open-loop control

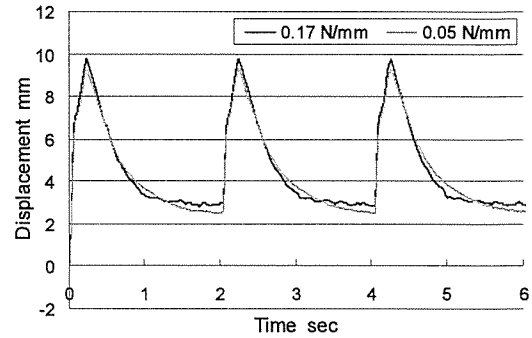

(b) Bias spring effect – PID control

Fig. 5 Changes in displacement obtained from the shape memory alloy fibre tested with the PID control under the different bias spring condition: a) open-loop, b) PID control.

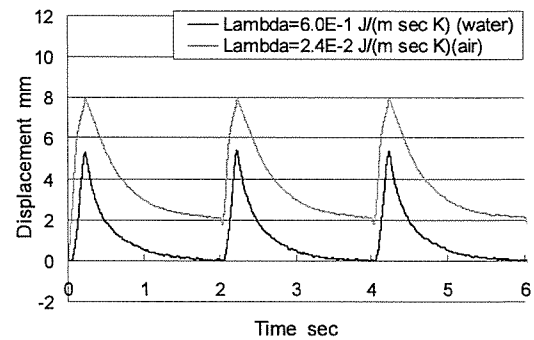

(a) Heat transfer effect – open-loop control

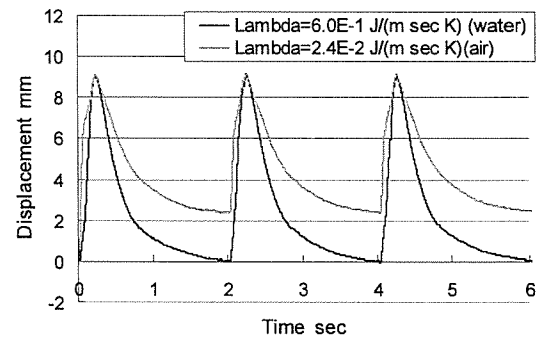

(b) Heat transfer effect – PID control

Fig. 6 Changes in displacement obtained from the shape memory alloy fibre tested with the PID control under the different ambient heat transfer condition: a) open-loop, b) PID control.

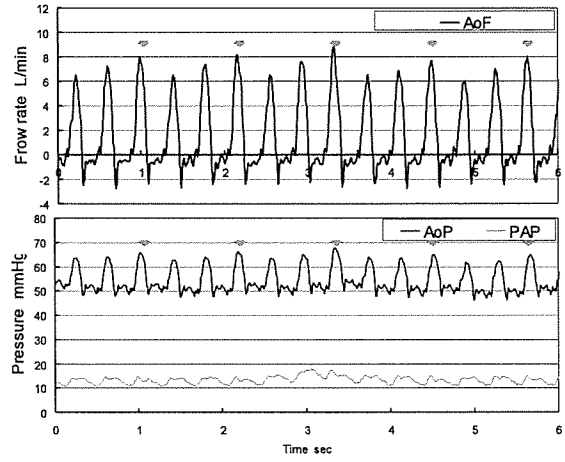

Fig. 7 Hemodynamic waveforms obtained from a goat; 'AoF': aortic flow at ascending aorta, 'AoP': aortic pressure measured at ascending aorta, 'PAP': pulmonary arterial pressure. The red arrows indicated the mechanical assistance by the artificial myocardial support.

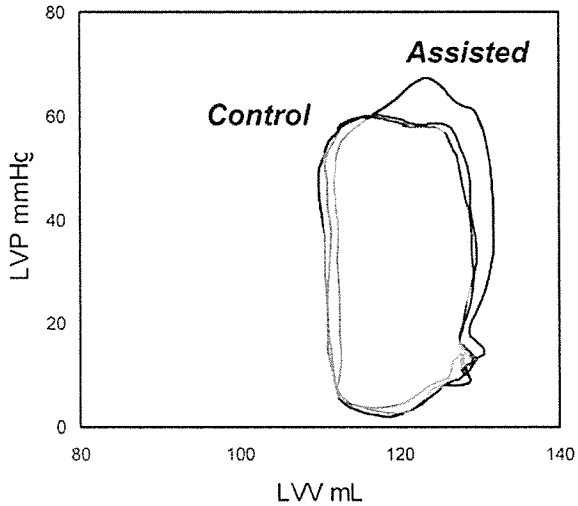

Fig. 8 Pressure-volume relationships obtained from a goat; 'Control': without assistance, 'Assisted': with mechanical assistance by the myocardial assist device developed.

ACKNOWLEDGEMENT

The authors would like to extend their appreciation to Mr. Kimio Kikuchi and Mr. Tomio Kumagai for their cooperation in the animal experiments. This study was supported by Grant in Aid for Scientific Research of Ministry of Health, Labour and Welfare (H17-nano-009), and Ministry of Education, Culture, Sports, Science and Technology (17790938). And this study was partly supported by Grant in Aid for Scientific Research of Pharmaceuticals and Medical Devices Agency (02-1).

REFERENCES

[1] HOSENPUD JD, et al. (1998): 'The registry of the international so-ciety for heart and lung transplantation: fifteenth offi-cial report–1998', J Heart Lung Transplant, 17, pp. 656–68.

[2] SHIMIZU T, et al. (2002): 'Fabrication of pulsatile cardiac tissue grafts using a novel 3-dimensional cell sheet manipulation technique and temperature-responsive cell culture surfaces', Circ Res, 90(3), e40.

[3] ANSTADT GL, et al. (1965): 'A new instrument for prolonged mechanical massage', Circulation, 31(Suppl. II), p.43.

[4] ANSTADT M, et al. (1991): 'Direct mechanical ventricular actruator', Resuscitation, 21, pp. 7-23.

[5] KAWAGUCHI O, et al. (1997): 'Dynamic cardiac compression improves contractile efficiency of the heart', J Thorac Cardiovasc Surg, 113, pp. 923-31.

[6] SAWYER PN, et al. (1976): 'Further study of NITINOL wire as contrctile artificial muscle for an artificial heart', Carrdiovasc Diseases Bull. Texas Heart Inst 3, p. 65.

[7] WESTABY S (2000): 'Non-transplant surgery for heart failure', Heart, 83: pp. 603–10

[8] SUMA H, et al. (2000): 'Non transplant cardiac surgery for end-stage cardiomyopathy', J Thorac Cardiovasc Surg, 119, pp. 1233–44.

[9] RAMAN JS, et al. (2005): 'The mid-term results of ventricular containment (Acorn Wrap) for end-stage ischemic cardiomyopathy',

[10] PILLA JJ, et al. (2002): 'Ventricular constraint using the cardiac support device reduces myocardial akinetic area in an ovine model of acute infarction', Circulation, 106[Suppl 1], I207-I211.

[11] BUEHLER WJ, GILFRICH J, WILEY KC (1963): 'Effect of low-temperature phase changes on the mechanical properties of alloys near composition TiNi', J Appl Phys, 34, p.1465.

[12] HOMMA D, MIWA Y, IGUCHI N, et al. (1982): 'Shape memory effect in Ti-Ni alloy during rapid heating," Proc of 25th Japan Congress on Materials Research.

[13] NITTA S, et al. (1983): 'Application of shape memory alloy for an artificial heart driving system', MBE 83-49, pp. 45-51 (in Japanese)

[14] YAMBE T, et al. (2004): 'Addition of rhythm to non-pulsatile circulation', Biomed Pharmacother, 58 Suppl 1:S145-9.

[15] YAMBE T, et al. (2004): 'Artificial myocardium with an artificial baroreflex system using nano technology', Biomed Pharmacother, 57 Suppl 1:122s-125s.

[16] WANG Q, et al. (2004): An artificial myocardium assist system: electrohydraulic ventricular actuation improves myocardial tissue perfusion in goats', Artif Organs, 28(9), pp. 853-857.

The American Journal of Pathology, Vol. 171, No. 4, October 2007

DOI: 10.2353/ajpath.2007.061191

Cardiovascular, Pulmonary and Renal Pathology

Macrophage Colony-Stimulating Factor Improves Cardiac Function after Ischemic Injury by Inducing Vascular Endothelial Growth Factor Production and Survival of Cardiomyocytes

Tatsuma Okazaki,* Satoru Ebihara,* Masanori Asada,* Shinsuke Yamanda,* Yoshifumi Saijo,† Yasuyuki Shiraishi,† Takae Ebihara,* Kaijun Niu,* He Mei,* Hiroyuki Arai,* and Tomoyuki Yambe†

From the Department of Geriatrics and Gerontology, Tohoku University School of Medicine, Sendai; and the Department of Medical Engineering and Cardiology,† Institute of Development, Aging, and Cancer, Tohoku University, Sendai, Japan*

Macrophage colony-stimulating factor (M-CSF), known as a hematopoietic growth factor, induces vascular endothelial growth factor (VEGF) production from skeletal muscles. However, the effects of M-CSF on cardiomyocytes have not been reported. Here, we show M-CSF increases VEGF production from cardiomyocytes, protects cardiomyocytes and myotubes from cell death, and improves cardiac function after ischemic injury. In mice, M-CSF increased VEGF production in hearts and in freshly isolated cardiomyocytes, which showed M-CSF receptor expression. In rat cell line H9c2 cardiomyocytes and myotubes, M-CSF induced VEGF production via the Akt signaling pathway, and M-CSF pretreatment protected these cells from H_2O_2-induced cell death. M-CSF activated Akt and extracellular signal-regulated kinase signaling pathways and up-regulated downstream anti-apoptotic Bcl-xL expression in these cells. Using goats as a large animal model of myocardial infarction, we found that M-CSF treatment after the onset of myocardial infarction by permanent coronary artery ligation promoted angiogenesis in ischemic hearts but did not reduce the infarct area. M-CSF pretreatment of the goat myocardial infarction model by coronary artery occlusion-reperfusion improved cardiac function, as assessed by hemodynamic parameters and echocardiography. These results suggest M-CSF might be a novel therapeutic agent for ischemic heart disease. *(Am J Pathol 2007, 171:1093–1103; DOI: 10.2353/ajpath.2007.061191)*

The administration of angiogenic growth factors such as vascular endothelial growth factor (VEGF) is an innovative strategy to treat myocardial ischemia. VEGF has been used in animal models and in clinical trials of myocardial ischemia to develop growth of collateral blood vessels and to promote myocardial perfusion, and its therapeutic potential has been reported.[1–3] Hematopoietic growth factors are potent therapeutic agents for myocardial infarction. Erythropoietin improved cardiac function after myocardial infarction.[4,5] Granulocyte colony-stimulating factor (G-CSF) improved cardiac function and prevented cardiac remodeling after myocardial infarction.[6] A combination of stem cell factor and G-CSF treatment improved cardiac function and survival after myocardial infarction.[7] Macrophage colony-stimulating factor (M-CSF) in combination with G-CSF improved ventricular function after myocardial infarction in rats, but few results were shown by M-CSF treatment alone, and their mechanism was not defined.[8] Moreover, to estimate growth factor-induced therapeutic angiogenesis in hearts, large animal models are necessary,[3] but the effects of M-CSF in large animal models have not been reported. M-CSF has been initially characterized as a hematopoietic growth factor, and has been used to prevent severe infections in myelosuppressed patients after cancer chemotherapy.[9,10] M-CSF stimulates the survival, prolifera-

Supported by the Ministry of Education, Science, and Culture (grants 15590795, 18014004, 17590777, and 18790528); the Ministry of Health, Labor, and Welfare of the Japanese Government (Grant for Longevity Science grants 16C-1 and 18C-7); and by the Program for Promotion of Fundamental Studies in Health Science of Organizing for Drug ADR Relief, R&D Promotion, and Product Review of Japan.

Accepted for publication June 27, 2007.

Current address of T.O.: Department of Anatomy, University of California–San Francisco, San Francisco, CA.

Address reprint requests to Satoru Ebihara, M.D., Ph.D., Department of Geriatrics and Gerontology, Tohoku University School of Medicine, Seiryo-machi 1-1, Aoba-ku, Sendai 980-8574, Japan. E-mail: s_ebihara@geriat.med.tohoku.ac.jp.

tion, and differentiation of cells from mononuclear phagocyte lineage.[11]

Expression of VEGF in the heart has been documented,[12,13] and cardiomyocytes have been reported as a major source of VEGF in the heart.[12] Skeletal muscles expressed VEGF,[13,14] and M-CSF increased VEGF production from skeletal muscles *in vivo* and *in vitro*,[14] but it is unknown whether M-CSF increases VEGF production from cardiomyocytes. M-CSF treatment increased serum VEGF levels in mice,[14] and the level was in the potentially therapeutic range that could treat ischemic diseases in human patients.[15]

Erythropoietin and G-CSF directly protected cardiomyocytes from cell death stimulation.[4,6] M-CSF improves the survival of mononuclear phagocyte lineage cells,[11] but the cell survival effect of M-CSF on cardiomyocytes is unknown. As for their signaling pathways, M-CSF activates Akt, extracellular signal-regulated kinase (ERK), and/or Janus-associated kinase (Jak)-signal transducer and activator of transcription (STAT) cell signaling pathways in bone marrow-derived macrophages and macrophage cell lines.[16–18] M-CSF increased VEGF production in skeletal muscles via Akt activation *in vitro*.[14] However, the cell signaling pathways of M-CSF in cardiomyocytes have not been investigated.

In the present study, we investigated the angiogenic and protective effects of M-CSF on cardiomyocytes *in vitro* and *in vivo*, in mice, rats, and goats. We show that M-CSF increases VEGF production in cardiomyocytes via Akt activation, directly protects cultured cardiomyocytes and myotubes from cell death stimulation by Akt and ERK activation and by up-regulation of downstream anti-apoptotic protein Bcl-xL. Moreover, we show the benefits of M-CSF treatment for ischemic heart diseases *in vivo* using goats as a large animal model.

Materials and Methods

Reagents and Cell Culture

Human M-CSF (Kyowa Hakko Kogyo, Tokyo, Japan) was dissolved in saline for goat experiments described below or in phosphate-buffered saline (PBS) for other experiments. Phycoerythrin-labeled anti-M-CSF receptor (M-CSF-R) monoclonal antibody, control rat IgG2a, and unlabeled anti-CD16/32 monoclonal antibody were purchased from eBioscience (San Diego, CA). H9c2 cells (American Type Culture Collection, Manassas, VA) were cultured in high-glucose Dulbecco's modified Eagle's medium containing 10% fetal calf serum, 100 U/ml penicillin, and 0.1 mg/ml streptomycin (growth medium, GM). To induce cardiac differentiation, H9c2 myoblasts were cultured in differentiation medium (DM) with daily supplementation of 10 nmol/L *all-trans*-retinoic acid (ATRA) (Sigma, St. Louis, MO), with medium changed every 2 days.[19] The difference between GM and DM is 1% fetal calf serum in DM. H9c2 myoblasts were differentiated to myotubes by culturing in the same DM for 11 days.[20] Mouse primary cardiomyocytes were obtained from 1- to 3-day-old neonatal C57BL/6 mice.[21] Heart ventricles were washed in ice-cold Hanks' balanced salt solution without either Ca^{2+} or Mg^{2+} and then minced. The cells were dissociated with 0.25% trypsin in Hanks' balanced salt solution. The supernatants were collected every 15 minutes and centrifuged. To exclude nonmuscle cells, the cells were cultured at 37°C for 2 hours. Then the suspended cells were collected and cultured at 1×10^5 cells/cm^2. After 48 hours, more than 90% of the cells were considered as cardiomyocytes by cross-striation structure staining with Bodipy FL phallacidin (Molecular Probes, Eugene, OR).

Cell Proliferation and Cell Death Assays

H9c2 cells (5×10^3 cells) were plated on 96-well plates and differentiated to cardiomyocytes or myotubes, and the assays were performed as previously shown.[22] For proliferation assays, H9c2 cardiomyocytes or myotubes were treated with M-CSF for indicated time periods, and the cell numbers were counted by a water-soluble tetrazolium (WST) assay using a cell counting kit (Dojindo, Tokyo, Japan). For cell death assays, differentiated H9c2 cells were incubated with M-CSF in the presence or absence of PD98059 (at 30 or 6 μmol/L; Biosource, Camarillo, CA) or LY294002 (at 10 or 2 μmol/L; Biosource) for 24 hours. Then the cells were stimulated with indicated amount of H_2O_2 for 8 hours. The cell viability was determined by the WST assay.

Flow Cytometry

The cells were incubated with unlabeled anti-CD16/32 monoclonal antibody to block nonspecific binding and then with phycoerythrin-labeled antibodies. Flow cytometry was performed with a FACScan (BD Bioscience, San Jose, CA).[14]

Histology

The goat hearts were fixed in 10% formalin, embedded in paraffin, and sectioned. The sections were stained with hematoxylin and eosin (H&E) or Masson's elastic stain. The microvessel density in myocardial infarction lesions was determined as previously shown by immunohistochemical staining of goat hearts with polyclonal rabbit anti-human factor VIII-related antigen antibody (DakoCytomation, Carpinteria, CA) at 1:200 dilution.[14,23] The applicability of this antibody to goats was previously reported.[24] The image with the highest microvessel density was chosen at ×100 magnification, and the vessels were counted at ×200 magnification. Two independent investigators counted at least four fields for each section, and the highest count was taken. To quantify the infarct area, a standard point-counting technique was used as previously described with minor modifications.[25] In brief, the whole heart cross section with highest infarct area was selected, and a 200-point grid was superimposed onto each captured image using Adobe Photoshop (Adobe Systems Inc., San Jose, CA). The area fraction of infarction was

calculated by dividing the number of infarct points by the total number of points falling on the tissue section and was expressed as a percentage.

Western Blot Analysis

Western blot analysis was performed as shown previously.[26] H9c2 myoblasts (5×10^5 cells) were cultured in GM on day 0. From day 1, the cells were differentiated to cardiomyocytes or myotubes. After differentiation, the cells were serum-starved for 6 hours and stimulated with M-CSF. For inhibitor experiments, the cells were cultured with inhibitors for 30 minutes and then stimulated with M-CSF and inhibitors. PD98059 was incubated at a concentration of 30 or 6 μmol/L, and LY294002 was incubated at a concentration of 10 or 2 μmol/L. The cell lysates were subjected to 12% sodium dodecyl sulfate-polyacrylamide gel electrophoresis and transferred onto polyvinylidene difluoride membranes (Millipore, Billerica, MA). The membranes were blotted with antibodies to phospho-ERK, phospho-Akt, phospho-Stat1, phospho-Stat3, phospho-Bad, Bcl-xL (Cell Signaling Technology, Beverly, MA), phospho-Jak1, or M-CSF-R (Santa Cruz Biotechnology, Santa Cruz, CA). The membranes blotted with antibodies to detect phosphorylation were then reblotted with antibodies to total ERK, Akt, Stat1, Stat3, Bad (Cell Signaling Technology), or Jak1 (Santa Cruz Biotechnology).

Mouse and Goat Preparation

The Laboratory Animal Committee at Tohoku University approved all animal experiments. Male C57BL/6 mice, 7 to 9 weeks old, were injected intramuscularly with M-CSF (200 μg/kg body weight) or PBS (control) for 3 consecutive days ($n = 5$ per group). Adult male goats (48 to 53 kg body weight) were intubated and anesthetized with 2% halothane as previously reported ($n = 3$ per group).[27] The goats were incised between the fourth and fifth ribs, and a left lateral thoracotomy was performed. Myocardial infarction was induced by left anterior descending coronary artery ligation with some modifications.[28] For the permanent left anterior descending coronary artery ligation model, left anterior descending coronary artery was ligated at a point ~60% from the beginning of the left coronary artery to the apex. M-CSF (40 μg/kg body weight) intravenous injection began just after the ligation and continued daily for 13 days; on day 14, the goats were anesthetized with 2% halothane and sacrificed. Control goats were injected with saline. For the ischemia-reperfusion model, M-CSF was injected intravenously for 3 consecutive days. Then the left anterior descending coronary artery was ligated at a point ~40% from the beginning of the left coronary artery to the apex for 30 minutes followed by reperfusion.[5] A micromanometer tipped catheter (Millar Instruments Inc., Houston, TX) was positioned in the left ventricle (LV). Hemodynamic parameters were recorded using a data recording unit (TEAC Corp., Tokyo, Japan) with sampling frequency of 1.5 kHz. Echocardiography was performed using a Sonos 5500 (Hewlett Packard, Andover, MA).

Enzyme-Linked Immunosorbent Assay (ELISA)

Mouse hearts were isolated, washed, homogenized in ice-cold PBS, and centrifuged. The protein level in the supernatant was adjusted to 10 mg/ml by the BCA protein assay kit (Pierce, Rockford, IL), and subjected to ELISA using a VEGF ELISA kit (R&D Systems, Minneapolis, MN). Carrageenan (Sigma) and rat anti-mouse CD11b monoclonal antibody (Serotec, Oxford, UK) treatment was performed as previously reported.[14] Culture medium of mouse primary cardiomyocytes (2×10^5 cells) was changed daily. H9c2 myoblasts (5×10^3 cells) were differentiated to cardiomyocytes or myotubes. H9c2 cardiomyocytes were incubated with M-CSF and ATRA in the presence or absence of LY294002 (10 μmol/L) for indicated time periods with daily culture medium change. H9c2 myotubes were cultured with M-CSF for indicated time periods. All of the supernatants were assayed by ELISA.

RNA Isolation and Reverse Transcriptase-Polymerase Chain Reaction (RT-PCR)

Total RNA was isolated using RNAzol B reagent (Tel-Test, Friendswood, TX). Placenta total RNA was purchased from BD Biosciences. Quantitative RT-PCR for VEGF and conventional RT-PCR for M-CSF-R were performed as previously shown.[14]

Data Analysis

Data are presented as mean ± SD. Statistical analysis was performed using analysis of variance with Fisher's least significant difference test. P values <0.05 were considered as significant.

Results

M-CSF Increases Heart VEGF Production in Vivo

Previous studies have shown that M-CSF increased VEGF production in skeletal muscles, and the heart expresses VEGF. Therefore, we examined whether M-CSF increases heart VEGF production. Mice were treated with M-CSF, and then the cytoplasmic RNA in heart was assessed by quantitative RT-PCR. M-CSF significantly increased VEGF mRNA expression level in the hearts by 221% (Figure 1A). M-CSF receptor (M-CSF-R) mRNA expression was confirmed by conventional RT-PCR, and placenta-derived mRNA was used as a positive control (Figure 1B). To confirm VEGF at the protein level, M-CSF was injected into mice. The hearts were isolated, and ELISA for VEGF was performed. VEGF was detected in controls (Figure 1C). M-CSF significantly increased VEGF in the hearts by 21% (Figure 1C). Because M-CSF induces VEGF production *in vitro* from human monocytes,[29] we sought to clarify whether cardiomyocytes or the monocytes/macrophages in the heart produced VEGF after M-CSF treatment. Mice were treated with carra-

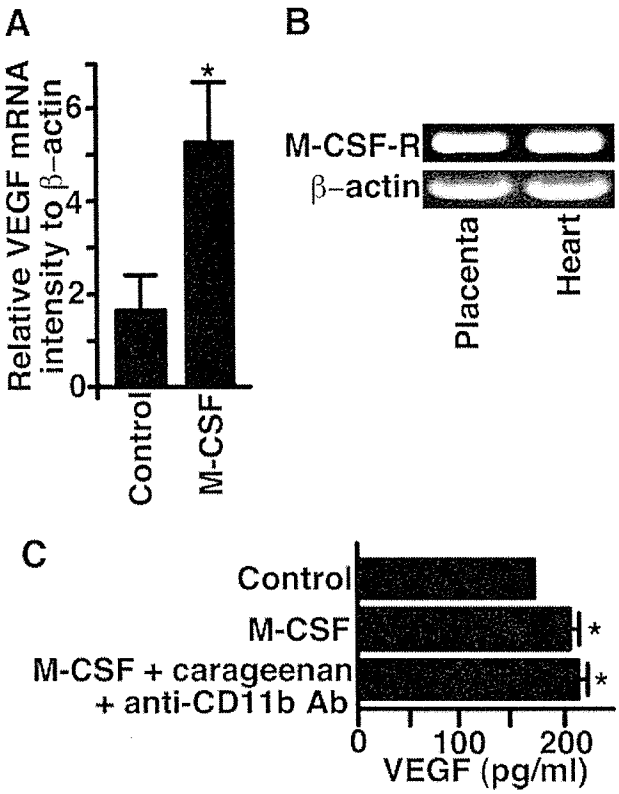

Figure 1. M-CSF increased heart VEGF production *in vivo*. Mice were injected intramuscularly with M-CSF (200 μg/kg) or PBS (control) for 3 consecutive days ($n = 5$ per group). **A:** Quantitative RT-PCR determined the VEGF mRNA expression. M-CSF treatment significantly increased the VEGF mRNA expression in hearts ($^*P < 0.05$). **B:** Conventional RT-PCR determined the M-CSF receptor (M-CSF-R) expression (top), and β-actin expression (bottom). **C:** The hearts were washed, homogenized in PBS, and centrifuged. ELISA determined the VEGF level in the supernatants containing 10 mg/ml protein. M-CSF significantly increased the VEGF level. M-CSF + carrageenan + anti-CD11b Ab indicates mice injected with carrageenin (1 mg) on days 1 and 4, with anti-CD11b monoclonal antibody (0.5 mg) on days 3 and 5, and with M-CSF on days 3, 4, and 5. On day 6, the hearts were isolated. This treatment did not affect the VEGF level ($^*P < 0.05$). Similar results were obtained from two independent experiments.

geenan and anti-CD11b monoclonal antibody to eliminate the monocytes/macrophages, as shown previously.[14] Macrophages were hardly observed in control mice hearts or in treated mice hearts (data not shown). The treatment did not affect M-CSF-induced VEGF production in the heart (Figure 1C).

M-CSF Increases VEGF Production by Cardiomyocytes in Vitro

To confirm the effect of M-CSF on heart VEGF production *in vitro*, mouse neonatal cardiomyocytes were isolated and stimulated with M-CSF. The culture medium was changed daily to maintain cell viability. Control cardiomyocytes produced VEGF, and M-CSF significantly increased the VEGF level on days 2 (by 10%) and 3 (by 31%) (Figure 2A). The M-CSF-R expression on cardiomyocytes was confirmed by fluorescence-activated cell sorting analysis (Figure 2B).

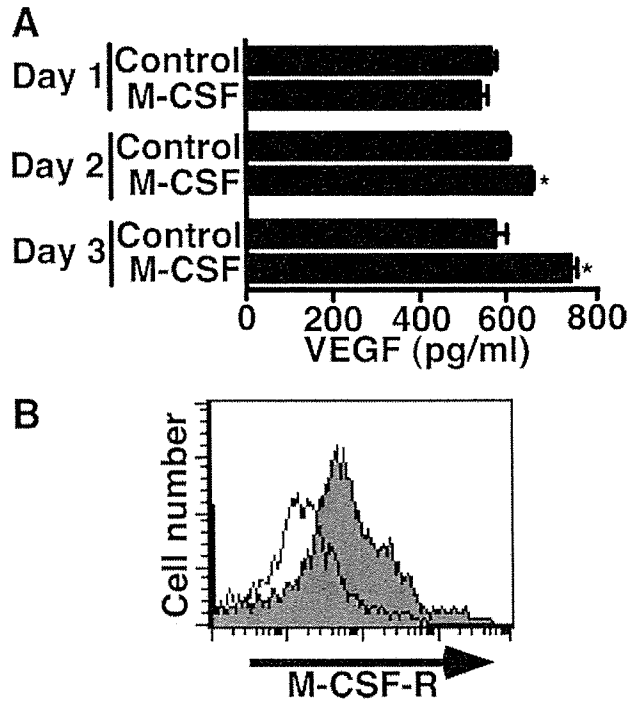

Figure 2. M-CSF enhanced heart VEGF production *in vitro*. **A:** Cultured cardiomyocytes from neonatal mice were stimulated with M-CSF (100 ng/ml) for the indicated time periods. Culture medium was changed daily, and the supernatants were subjected to ELISA. M-CSF significantly enhanced VEGF production on days 2 and 3 ($^*P < 0.01$). **B:** Cultured cardiomyocytes from neonatal mice expressed M-CSF-R. The shaded histogram indicates staining with M-CSF-R, and the blank histogram indicates background staining with control IgG. Similar results were obtained from two independent experiments.

M-CSF Increases VEGF Production from Differentiated H9c2 Cells

To investigate the effects of M-CSF on cardiomyocytes more precisely, rat H9c2 myoblast cells were differentiated to cardiomyocytes. H9c2 myoblasts differentiate to cardiomyocytes when they are cultured in DM with ATRA.[19] After differentiation, DM with ATRA was changed daily to maintain cell viability. VEGF was detected in supernatants from controls, and M-CSF increased H9c2 cardiomyocyte VEGF production on days 2 (by 10%) and 3 (by 20%) (Figure 3A). M-CSF increased skeletal muscle VEGF production.[14] H9c2 myoblasts cultured in the DM without ATRA for 11 days differentiate to H9c2 myotubes.[20] After differentiation, H9c2 myotubes were treated with M-CSF. H9c2 myotubes produced VEGF, and M-CSF significantly enhanced VEGF production on day 8 by 29% (Figure 3B).

M-CSF Protects Differentiated H9c2 Cells from H_2O_2-Induced Cell Death

Because M-CSF increased VEGF production from differentiated H9c2 cells, we investigated whether M-CSF increased the H9c2 cardiomyocyte cell number and found that it did not (Figure 4A). Similar results were obtained from the H9c2 myotubes (Figure 4A). M-CSF improves the survival of the mononuclear phagocyte lineage

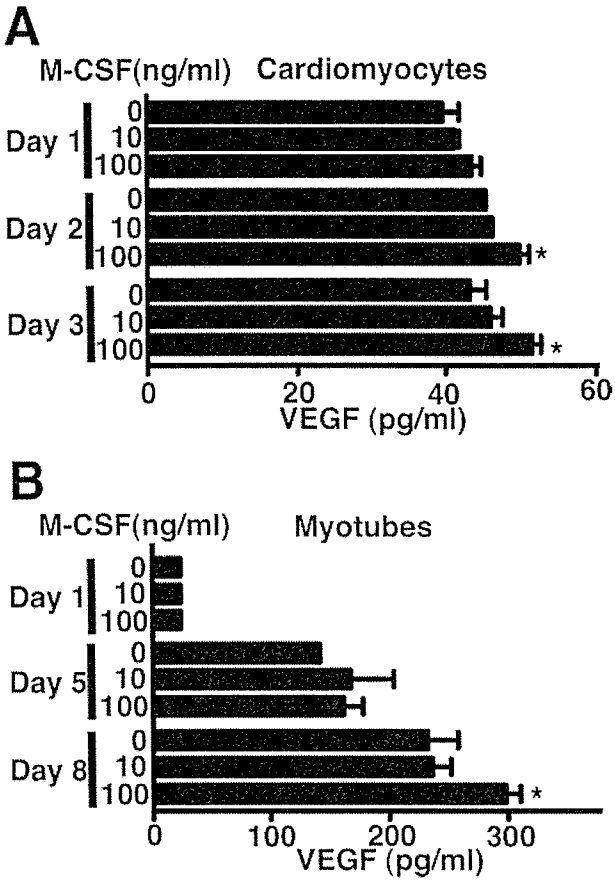

Figure 3. M-CSF increased VEGF production in differentiated H9c2 cells. **A:** H9c2 myoblasts cultured in DM (changed every 2 days) with daily supplementation of 10 nmol/L ATRA for 7 days were differentiated to H9c2 cardiomyocytes. The cells were stimulated with the indicated amount of M-CSF for indicated time periods. The culture medium was changed daily, and ELISA determined the VEGF level in the supernatant. M-CSF (100 ng/ml) increased VEGF production on days 2 and 3 ($^*P < 0.05$). **B:** H9c2 myoblasts cultured in the same DM for 11 days were differentiated to H9c2 myotubes. Then the cells were stimulated with the indicated amount of M-CSF for the indicated time periods without medium change. M-CSF (100 ng/ml) significantly increased VEGF production on day 8 ($^*P < 0.03$). Similar results were obtained from three independent experiments.

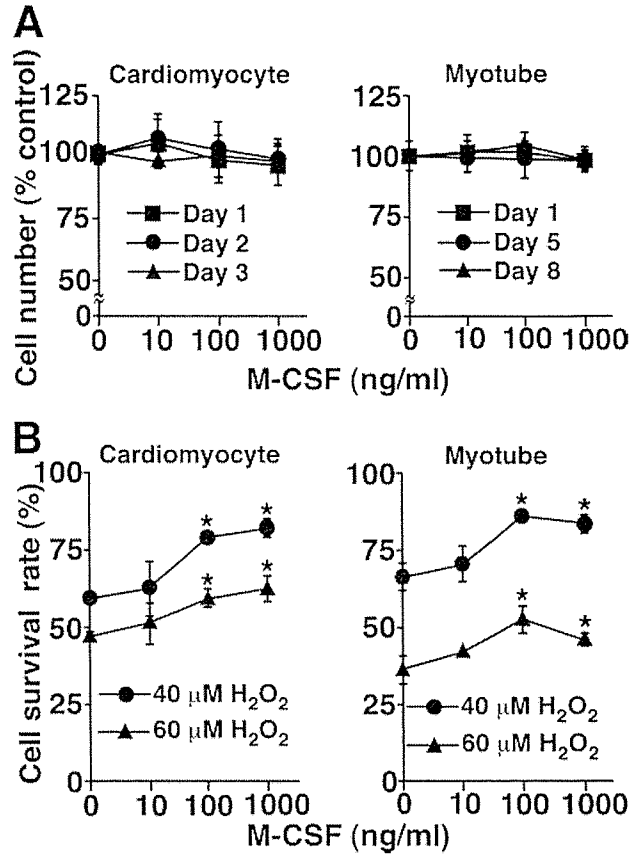

Figure 4. M-CSF protects differentiated H9c2 cells from H_2O_2-induced cell death. **A:** H9c2 cardiomyocytes were cultured with the indicated amount of M-CSF and ATRA for the indicated time periods, and the culture medium was changed daily. H9c2 myotubes were cultured with the indicated amount of M-CSF for the indicated time periods. WST assay determined the cell number. **B:** H9c2 cardiomyocytes or H9c2 myotubes were cultured with the indicated amount of M-CSF for 24 hours and then stimulated with H_2O_2 (40 or 60 μmol/L) for 8 hours. The culture medium of H9c2 cardiomyocytes was supplemented with ATRA. WST assay determined the cell viability. M-CSF (100 and 1000 ng/ml) significantly protected the cells from H_2O_2-induced cell death ($^*P < 0.03$). Similar results were obtained from three independent experiments.

cells.[11] Therefore, the cell survival effect of M-CSF on differentiated H9c2 cells from cytotoxic H_2O_2 exposure was examined. H9c2 cardiomyocytes were incubated with M-CSF and then exposed to H_2O_2. M-CSF significantly protected H9c2 cardiomyocytes from H_2O_2-induced cell death (Figure 4B). Similar results were obtained from H9c2 myotubes (Figure 4B).

M-CSF Activates ERK and Akt Signaling Pathways and Increases Bcl-xL Expression in Differentiated H9c2 Cells

The cell signaling pathways of M-CSF in cardiomyocytes and H9c2 myotubes have not been investigated. To elucidate molecular mechanisms of the M-CSF-induced cell survival, differentiated H9c2 cells were treated with M-CSF and then activation of ERK, Akt, and Jak-STAT signaling pathways was investigated. Western blot analysis showed two forms of M-CSF-R in differentiated H9c2 cells (Figure 5, A and C).[30] In H9c2 cardiomyocytes, M-CSF induced ERK activation, as indicated by its protein phosphorylation, whereas the protein levels of the total ERK in cell lysates were not different (Figure 5A). M-CSF activated the Akt, but M-CSF did not activate Jak1, Stat1, or Stat3 (Figure 5A). ERK activation protects cardiomyocytes from cell death by up-regulating the anti-apoptotic protein Bcl-xL and inactivating the apoptotic protein Bad by its phosphorylation at Ser112.[31,32] Akt activation improves cardiomyocyte survival, but the main downstream signaling pathways of Akt for cardiomyocytes survival has not been clarified.[33] To clarify the target molecules of ERK in H9c2 cardiomyocytes, Bcl-xL expression was examined. Bcl-xL was detected in cells without M-CSF stimulation (Figure 5B). M-CSF up-regulated Bcl-xL expression, which peaked at 24 and 48 hours (Figure 5B). M-CSF did not phosphorylate Bad at Ser112 (Figure 5B). These results suggest M-CSF protected H9c2 cardiomyocytes by activating Akt and up-regulating Bcl-xL expression through ERK activation. In H9c2 myotubes, M-CSF activated ERK and Akt but did not activate Jak1 or Stat3

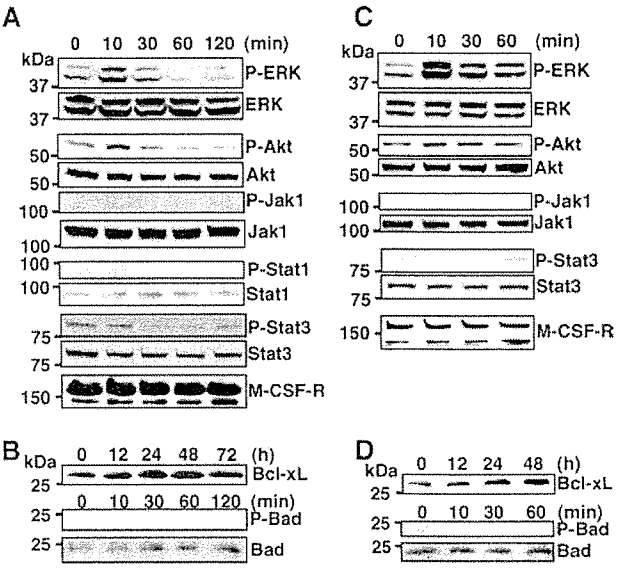

Figure 5. M-CSF activated ERK, Akt, and up-regulated Bcl-xL expression in differentiated H9c2 cells. H9c2 cardiomyocytes (**A** and **B**) or H9c2 myotubes (**C** and **D**) were stimulated with M-CSF (100 ng/ml) for the indicated time periods, and then the cell lysates were blotted with antibodies specific for the activated form of ERK (phospho-ERK), Akt (phospho-Akt), Jak1 (phospho-Jak1), Stat1 (phospho-Stat1), Stat3 (phospho-Stat3), or phosphorylated Bad (phospho-Bad). The membranes were reblotted with antibodies to total ERK, Akt, Jak1, Stat1, Stat3, or Bad, respectively. Expression of M-CSF-R or Bcl-xL was confirmed by blotting the membrane with specific antibodies. Similar results were obtained from three independent experiments.

(Figure 5C). M-CSF gradually up-regulated Bcl-xL expression until 48 hours (Figure 5D) but did not phosphorylate Bad at Ser112 (Figure 5D).

The Role of M-CSF-Induced Akt and ERK Activation in VEGF Production and Cell Survival in Differentiated H9c2 Cells

M-CSF increases VEGF production through Akt activation in skeletal muscles. To determine the role of Akt activation in H9c2 cardiomyocytes VEGF production, H9c2 cardiomyocytes were treated with Akt-specific inhibitor LY294002, and the culture supernatant was assayed by ELISA. LY294002 and M-CSF treatment for 2 days significantly impaired VEGF production in H9c2 cardiomyocytes (Figure 6A). LY294002 and M-CSF treatment for 3 days further decreased VEGF production, and the VEGF level became less than the detection level (Figure 6A). To determine the role of ERK and Akt activation after M-CSF treatment in differentiated H9c2 cell survival, differentiated H9c2 cells were treated with LY294002 or the ERK-specific inhibitor PD98059. PD98059 inhibited ERK activation and LY294002 inhibited Akt activation in H9c2 cardiomyocytes (Figure 6B). Similar results were obtained from H9c2 myotubes (data not shown). PD98059 enhanced H_2O_2-induced cell death of H9c2 cardiomyocytes (Figure 6C). The protective effect of M-CSF was impaired by PD98059; however, M-CSF significantly protected H9c2 cardiomyocytes from cell death (Figure 6C). A similar result was obtained from LY294002 in H9c2 cardiomyocytes (Figure 6C). In H9c2 myotubes, PD 98059 enhanced H_2O_2-induced cell death, and PD98059

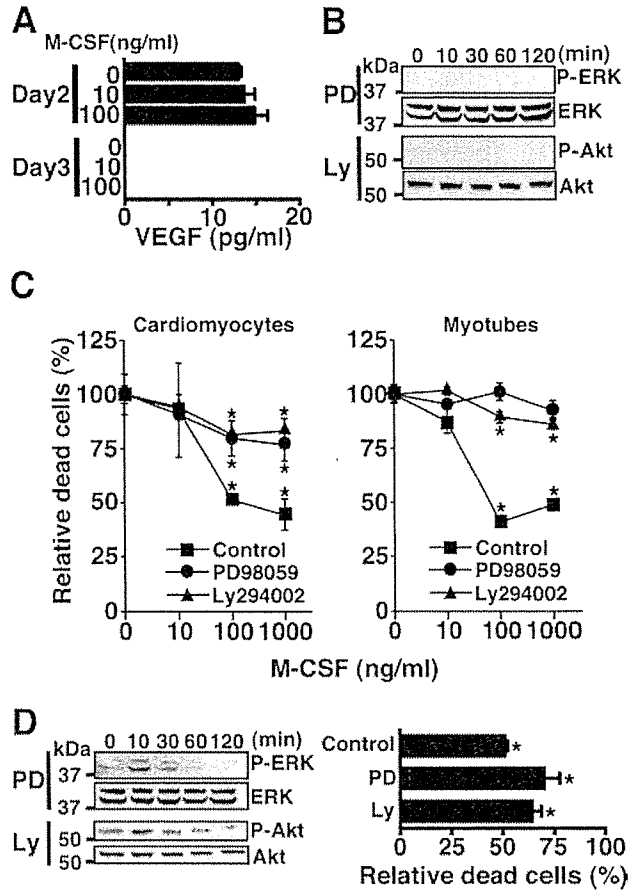

Figure 6. The role of M-CSF-induced Akt and ERK activation in VEGF production and cell protection in differentiated H9c2 cells. **A:** H9c2 cardiomyocytes were cultured with M-CSF and 10 μmol/L LY294002 for the indicated time periods. The culture medium was changed daily and ELISA determined the VEGF level. **B:** H9c2 cardiomyocytes were incubated with 30 μmol/L PD98059 (PD) or 10 μmol/L LY294002 (Ly) for 30 minutes, then stimulated with M-CSF (100 ng/ml) and inhibitors, and analyzed as described in Figure 5. **C:** Differentiated H9c2 cells were stimulated with indicated amount of M-CSF with PD98059 (30 μmol/L) or LY294002 (10 μmol/L) for 24 hours. Then the cells were stimulated with H_2O_2 (40 μmol/L) for 8 hours, and WST assay determined the dead cells. M-CSF (0 ng/ml) in each group is considered as 100%, and relative cell death rates in each group are shown. $^*P < 0.03$ compared with 0 ng/ml M-CSF in each group. Similar results were obtained from three independent experiments. **D:** H9c2 cardiomyocytes were incubated with reduced concentrations of PD98059 (6 μmol/L) or LY294002 (2 μmol/L). Left: H9c2 cardiomyocytes were treated with PD98059 or LY294002 for 30 minutes, stimulated with M-CSF (100 ng/ml) and inhibitors, and then analyzed as described in Figure 5. Right: H9c2 cardiomyocytes were treated with PD98059, LY294002, or without inhibitors (control) with (100 ng/ml) or without (0 ng/ml) M-CSF for 24 hours. Then the cells were stimulated with H_2O_2 (40 μmol/L) for 8 hours, and dead cells were assessed by WST assay. In each inhibitor group, dead cells at 0 ng/ml M-CSF are considered as 100%, and relative cell death rates at 100 to 0 ng/ml M-CSF in each inhibitor group are shown. $^*P < 0.02$ compared with 0 ng/ml M-CSF in each group.

abolished the protective effect of M-CSF (Figure 6C). LY294002 enhanced H_2O_2-induced cell death in H9c2 myotubes; however, M-CSF significantly protected H9c2 myotubes from cell death (Figure 6C). Moreover, a dose-response experiment of PD98059 or LY294002 was performed to observe ERK or Akt phosphorylation and cellular survival of H9c2 cardiomyocytes (Figure 6D). Similar results were obtained from H9c2 myotubes (data not shown). VEGF protected myogenic cells from cell death.[34] To confirm whether the cell survival effect of M-CSF de-

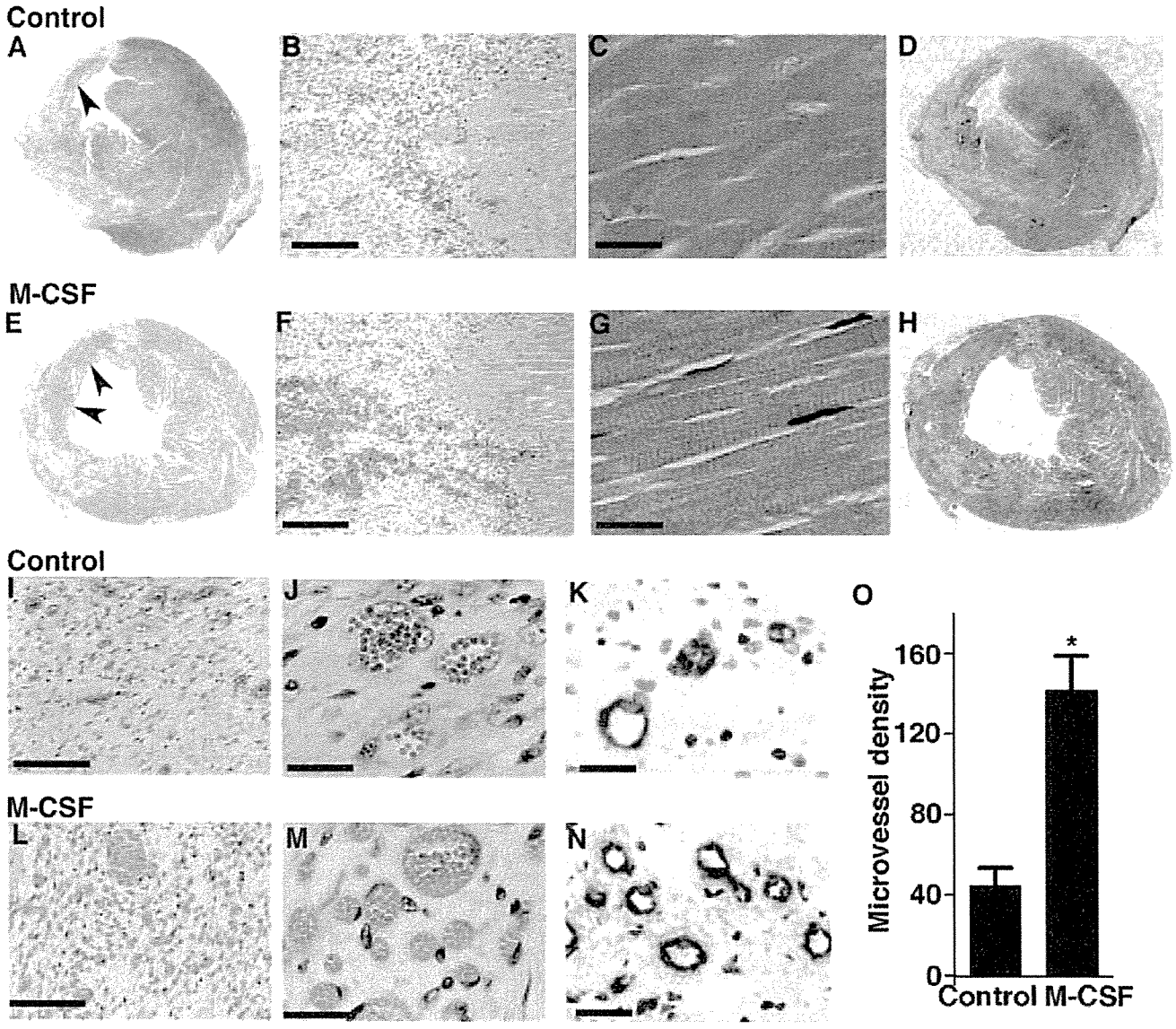

Figure 7. M-CSF promotes angiogenesis in goat heart after myocardial infarction. The goat left anterior descending coronary artery was permanently ligated, and the goats were sacrificed on day 14. M-CSF indicates goats intravenously injected with M-CSF shortly after the coronary artery ligation daily until day 13. Controls were injected with saline. Paraffin sections were stained with H&E (**A–C**, **E–G**, **I**, **J**, **L**, and **M**), Masson's elastic stain (**D** and **H**), and anti-factor VIII-related antigen antibody (**K** and **N**). **A** and **E:** Left anterior descending coronary artery ligation induced myocardial infarction. **Arrowheads** indicate cardiomyocytes in ischemic lesions. (**B**, **C**, **F**, and **G**) Microscopic observations indicated the cardiomyocytes in the ischemic lesions were dead. **D** and **H:** The green staining indicates fibrosis or scars in hearts. **I**, **J**, **L**, and **M:** The microvessels in ischemic lesions. **K** and **N:** The microvessels in ischemic lesions were immunohistochemically stained with anti-factor VIII-related antigen antibody. **O:** M-CSF significantly increased microvessel density in ischemic lesions ($^*P < 0.01$, $n = 3$ per group). The images represent one of three goats in each group. Scale bars: 200 μm (**B** and **F**); 20 μm (**C**, **G**, **J**, **K**, **M**, and **N**); 100 μm (**I** and **L**).

pends on VEGF, H9c2 cardiomyocytes and myotubes were cultured with an anti-VEGF antibody and M-CSF. Incubation with anti-VEGF antibody did not impair the cell protective effect of M-CSF from H_2O_2 stimulation suggesting that the effect of M-CSF was not VEGF-dependent (data not shown).

M-CSF Promotes Angiogenesis in Goat Ischemic Heart after Permanent Coronary Artery Ligation

M-CSF treatment elevated systemic VEGF level in mice from a nondetectable level to potentially therapeutic levels.[14,15] The cell protective and angiogenic effects of M-CSF *in vivo* were examined using goats as a large animal model for myocardial infarction. Large animal models are necessary for evaluating growth factor-induced therapeutic angiogenesis,[3] and we have used goats for developing artificial heart devices.[27] We induced myocardial infarction by permanent left anterior descending coronary artery ligation. The coronary artery ligation resulted in LV infarction (Figure 7, A, D, E, and H). Macroscopically, M-CSF seemed to promote cardiomyocyte cell survival in ischemic lesions in comparison to the controls (Figure 7, A and E; arrowheads). Microscopy indicated that cardiomyocytes in ischemic lesions were dead cells in the controls (Figure 7, B and C). At low magnification, M-CSF seemed to protect cardiomyocytes from cell death in ischemic lesions (Figure 7F). However,

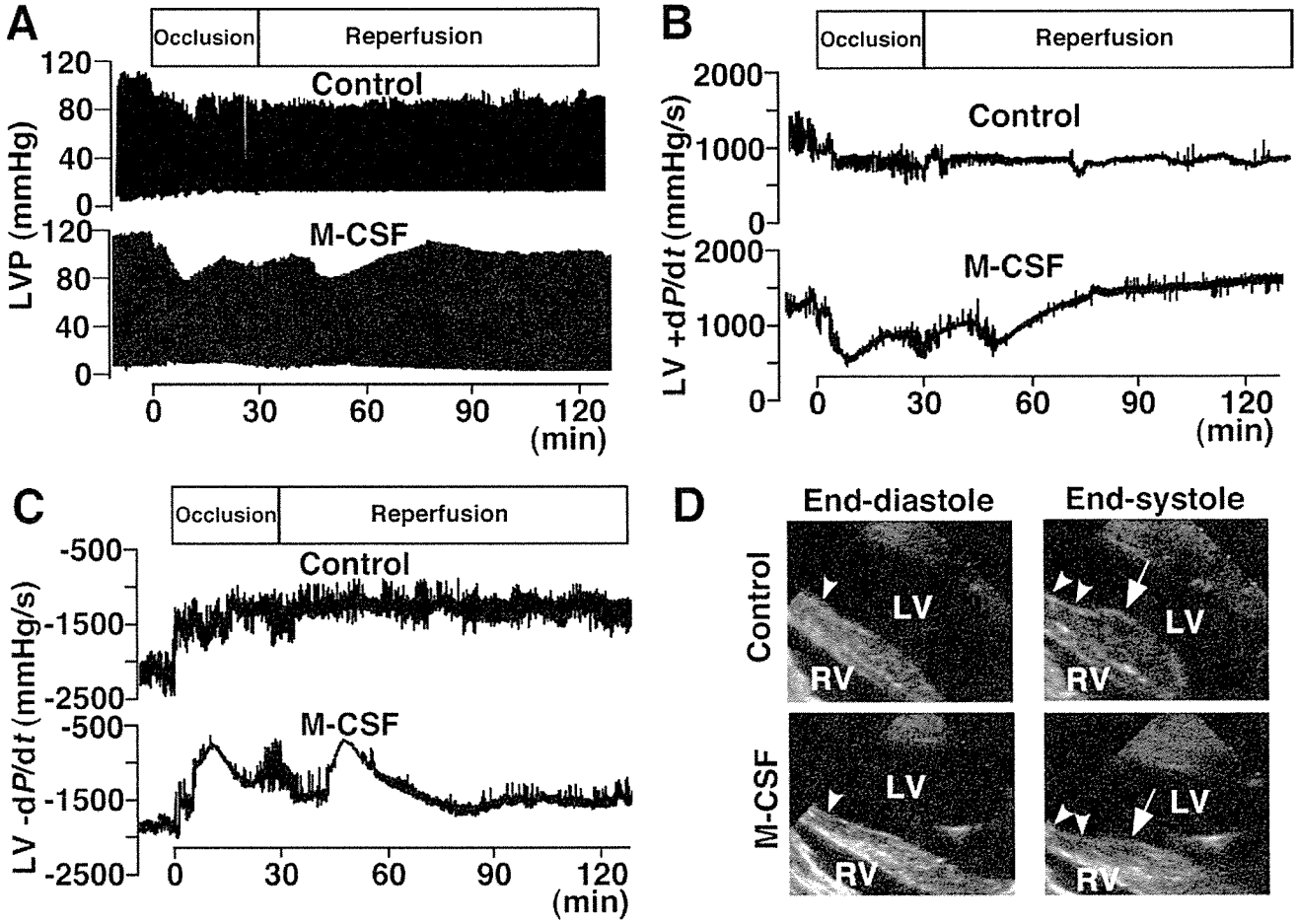

Figure 8. M-CSF pretreatment improved cardiac function after ischemic injury. M-CSF indicates goats intravenously injected with M-CSF daily for 3 days, whereas the control indicates goats injected with saline. The goat left anterior descending coronary artery was occluded for 30 minutes and then reperfused. **A–C:** Hemodynamic parameters before and during 30 minutes of left anterior descending coronary artery occlusion followed by 90 minutes of reperfusion are shown. Representative LVP records (**A**), representative positive dP/dt (**B**), and representative negative dP/dt (**C**) of control and M-CSF-treated goats. LVEDP, positive and negative dP/dt recovered in M-CSF-treated goats after reperfusion. **D: Arrowheads** indicate infarct areas. Compare **arrows**, which indicate wall contraction of nonischemic area at end systole, to **arrowheads**. In the infarct area, echocardiography shows dyskinetic wall movement in controls, whereas akinetic wall movement is shown in M-CSF-treated goats. Data are representative of three goats in each group.

at high magnification, most of the cardiomyocytes were dead (Figure 7G). Microvessels were observed in the ischemic lesions of control goats (Figure 7, I and J), and M-CSF treatment increased the number of microvessels (Figure 7, L and M). To confirm the microvessel density, we immunohistochemically stained goat hearts with anti-factor VIII-related antigen antibody (Figure 8, K and N).[23,24] M-CSF significantly increased microvessel density in ischemic lesions by 226% (Figure 7O). These results suggest that M-CSF promoted angiogenesis and induced collateral blood vessels in the ischemic heart. The infarct area quantification showed no significant difference between control and M-CSF-treated goats (controls, 30.4 ± 5.2%; M-CSF, 24.3 ± 2.1%). The residual presence of nuclei and cross striations in dead cardiomyocytes in ischemic lesions by M-CSF treatment (Figure 7G) suggests that the cardiomyocytes survived longer than control cardiomyocytes (Figure 7, C and G), but M-CSF-induced new vessels could not reach cardiomyocytes in ischemic lesions before their death.

M-CSF Pretreatment Improved Cardiac Function after Ischemic Injury Induced by Coronary Artery Occlusion-Reperfusion

Erythropoietin treatment did not change the infarct size, but it improved cardiac function in the rat coronary artery occlusion-reperfusion model.[5] Pretreatment with stem cell factor and G-CSF improved cardiac function after myocardial infarction.[7] To confirm further the effects of M-CSF in myocardial infarction, goats were pretreated with M-CSF for 3 days, and then myocardial infarction was induced by 30-minute left anterior descending coronary artery occlusion followed by reperfusion.[5,35] Cardiac function was assessed by measuring hemodynamic parameters using catheterization analysis and examining echocardiography. Echocardiographic examination showed no significant differences in basal findings in cardiac function in both groups. Catheterization analysis showed the LV pressure (LVP) records of control and M-CSF-treated goats (Figure 8A). LV end diastolic pressure

(LVEDP), which can influence overall cardiac function,[4] increased after the left anterior descending coronary artery occlusion in both groups. In controls, the LVEDP did not recover after reperfusion, but in M-CSF-treated goats, the LVEDP gradually recovered after reperfusion (Figure 8A), and at 90 minutes after the reperfusion, the LVEDP of M-CSF treated goats was significantly better than that of control goats (controls, 10.62 ± 0.98 mmHg; M-CSF, 7.61 ± 0.83 mmHg; $P < 0.02$). Positive and negative dP/dt are measures of overall cardiac contractility and relaxation, respectively.[4] Positive dP/dt decreased after the left anterior descending coronary artery occlusion both in control and M-CSF-treated goats (Figure 8B). After reperfusion, positive dP/dt did not recover in control goats (Figure 8B). In M-CSF treated goats, positive dP/dt gradually recovered after reperfusion and finally reached similar dP/dt levels before the occlusion (Figure 8B). At 90 minutes after the reperfusion, the positive dP/dt of M-CSF-treated goats was significantly better than that of control goats (controls, 886 ± 103 mmHg; M-CSF, 1506 ± 125 mmHg; $P < 0.01$). Moreover, recovery of negative dP/dt after left anterior descending coronary artery occlusion-reperfusion was observed only in M-CSF-treated goats (Figure 8C). At 90 minutes after the reperfusion, the negative dP/dt of M-CSF-treated goats was significantly better than that of control goats (controls, −1342 ± 92 mmHg; M-CSF, −1570 ± 108 mmHg; $P < 0.05$). Echocardiographic examination showed a paradoxical LV wall movement area indicated as a dyskinetic area after left anterior descending coronary artery occlusion in control goats (Figure 8D). In M-CSF-treated goats, echocardiography showed a LV wall movement arrest area indicated as an akinetic area after left anterior descending coronary artery occlusion, and a dyskinetic area could not be found (Figure 8D). In control hearts, the nonischemic wall contractions at end systole were enhanced. This suggested substitutive wall movement for the dyskinetic area to keep cardiac output (Figure 8D). These echocardiographic findings suggest improvement of LV wall movement in M-CSF-treated goats during left anterior descending coronary artery occlusion-reperfusion. The LV ejection fraction (LVEF) was evaluated by echocardiography, but LVEF did not significantly change between before and after the occlusion; therefore, LVEF between controls and M-CSF-treated ones were not compared. Recovery of LVEDP, positive and negative d*P*/d*t* after reperfusion, and improvement of LV wall movement during the left anterior descending coronary artery occlusion-reperfusion suggest M-CSF pretreatment improved cardiac function after ischemic injury.

Discussion

In this study, M-CSF increased VEGF production in hearts both *in vivo* and *in vitro*. *In vitro*, M-CSF increased VEGF production through Akt activation. Moreover, M-CSF directly protected cardiomyocytes from cell death by activating Akt and ERK resulting in up-regulation of the downstream anti-apoptotic protein Bcl-xL. M-CSF-R expression in the heart was shown both *in vivo* and *in vitro*, and these results suggest that the expression is functional. Similar cell-protective effects of M-CSF on H9c2 myotubes were shown. *In vivo*, M-CSF treatment after the onset of myocardial infarction promoted angiogenesis in the ischemic heart, suggesting development of collateral blood vessels. Furthermore, M-CSF pretreatment in the goat myocardial infarction model improves cardiac function, as indicated by improvement of LVEDP, positive and negative dP/dt, and LV wall movements.

Recent studies indicate intramyocardial transfer of plasmid or adenoviral DNA-encoding human VEGF has favorable effects in myocardial infarction animal models and in patients with coronary artery diseases.[1,2,36] Similar to these VEGF transfer strategies, M-CSF directly up-regulated VEGF production in cardiomyocytes. In addition, M-CSF significantly induced an increase in plasma VEGF in mice to therapeutic levels that induced therapeutic angiogenesis.[14,35] Therapeutic plasmid gene delivery to a target organ is difficult and often temporary. However, M-CSF treatment was easily achieved by peripheral intravenous or intramuscular injection. These data indicate a therapeutic potential of M-CSF in ischemic heart diseases. Basic fibroblast growth factor and hepatocyte growth factor have also been applied to therapeutic angiogenesis.[37] We treated mice with M-CSF and examined basic fibroblast growth factor and hepatocyte growth factor mRNA levels by quantitative RT-PCR. M-CSF did not increase basic fibroblast growth factor or hepatocyte growth factor mRNA levels in the heart (data not shown). We also examined plasma G-CSF level after M-CSF treatment in mice by ELISA. M-CSF did not increase plasma G-CSF level. However, there is still a possibility that M-CSF induces other factors that are responsible for the effects shown in this article.

Very recently, M-CSF was reported to accelerate infarct repair and attenuate LV dysfunction in rats.[35] However, these authors did not investigate VEGF induction or the cardioprotective effects of M-CSF and did not use a large animal model. In the present study, in the M-CSF-treated group, we observed an increase in microvessel density, increased presence of dead cardiomyocytes, and decreased presence of granuloma in ischemic lesions. The increased presence of dead cardiomyocytes in ischemic lesions and improvement of cardiac function after ischemia in M-CSF-treated goats suggest a longer survival of cardiomyocytes in M-CSF-treated goats than in the controls. This finding and the decreased presence of granuloma suggest that M-CSF reduced the progression rate of ischemic injury in ischemic hearts *in vivo*.

In human monocytes, LY294002 suppressed M-CSF-induced ERK activation.[38] This mechanism was explained as M-CSF stimulation-induced reactive oxygen species, which activated ERK. The addition of Akt inhibitor prevented reactive oxygen species production and thus suppressed ERK activation in M-CSF-stimulated monocytes.[38] In murine myeloid cell line FDC-P1, LY294002 suppressed M-CSF-induced ERK activation, but it was not significant.[39] In H9c2 cardiomyocytes, LY294002 seemed to impair ERK activation in part. To suggest the involvement of Akt in M-CSF-induced ERK

activation in cardiomyocytes, we may have to use other Akt-inhibiting methods, as this time we could not reach a clear conclusion. For VEGF production, PD98059 treatment for 1 day did not affect M-CSF-induced VEGF production in differentiated H9c2 cells, whereas LY294002 treatment impaired M-CSF-induced VEGF production, suggesting M-CSF-induced VEGF production in differentiated H9c2 cells were Akt-dependent. This is the first report that suggested the presence of signal transduction pathways in cardiomyocytes in response to M-CSF. Further experiments are required for pursuing the M-CSF-induced intracellular signaling pathways in cardiomyocytes or in myotubes.

Goat hearts have a left coronary artery-dominant blood supply.[40] The goat coronary artery anatomy was remarkably regular, and coronary artery collaterals could not be demonstrated,[40] indicating frailty after heart ischemic injury. For the left anterior descending coronary artery occlusion-reperfusion model, the goat left anterior descending coronary artery was ligated at a point ~40% from the beginning of the left coronary artery to the apex, but LVEF decrease could not be detected by echocardiography. Occlusion of a more proximal site of goat left anterior descending coronary artery has been reported to be invariably fatal,[40] and our preliminary experiments with a more proximal left anterior descending coronary artery ligation supported this finding. Therefore, using goats, LVEF after myocardial infarction could not be evaluated. We were not able to assess plasma VEGF and the involvement of bone marrow-derived cells in the goat model because the appropriate reagents are not commercially available. We could not find a staining method specific for cardiomyocyte viability in goat hearts. Infarct area quantification suggested a trend that M-CSF might decrease infarct area. However, infarct area quantification showed no significant difference in control and M-CSF-treated goat hearts. Further investigation is required to clarify the roles and mechanisms of M-CSF in ischemic diseases using other species and other M-CSF treatment protocols.

The cell-protective and VEGF-inducing effects of M-CSF both in cardiomyocytes and myotubes were shown, and the effects were confirmed by improvement of cardiac function and activated angiogenesis in goat ischemic hearts. M-CSF is already in use clinically, and data from patients such as side effects are accumulating. Moreover, M-CSF administration is easily performed with minimal invasiveness in human patients. In this study, we showed the potential benefits of M-CSF treatment and its new mechanisms in ischemic heart diseases.

Acknowledgments

We thank Peter Baluk, Hiroya Hashizume, Hiroshi Kubo, and Katsutoshi Nakayama for helpful comments on the manuscript; and Amy Ni and Shannon Freeman for correcting the manuscript.

References

1. Yoon YS, Johnson IA, Park JS, Diaz L, Losordo DW: Therapeutic myocardial angiogenesis with vascular endothelial growth factors. Mol Cell Biochem 2004, 264:63–74
2. Kastrup J, Jorgensen E, Ruck A, Tagil K, Glogar D, Ruzyllo W, Botker HE, Dudek D, Drvota V, Hesse B, Thuesen L, Blomberg P, Gyongyosi M, Sylven C: Direct intramyocardial plasmid vascular endothelial growth factor-A165 gene therapy in patients with stable severe angina pectoris A randomized double-blind placebo-controlled study: the Euroinject One trial. J Am Coll Cardiol 2005, 45:982–988
3. Markkanen JE, Rissanen TT, Kivela A, Yla-Herttuala S: Growth factor-induced therapeutic angiogenesis and arteriogenesis in the heart-gene therapy. Cardiovasc Res 2005, 65:656–664
4. Parsa CJ, Matsumoto A, Kim J, Riel RU, Pascal LS, Walton GB, Thompson RB, Petrofski JA, Annex BH, Stamler JS, Koch WJ: A novel protective effect of erythropoietin in the infarcted heart. J Clin Invest 2003, 112:999–1007
5. Calvillo L, Latini R, Kajstura J, Leri A, Anversa P, Ghezzi P, Salio M, Cerami A, Brines M: Recombinant human erythropoietin protects the myocardium from ischemia-reperfusion injury and promotes beneficial remodeling. Proc Natl Acad Sci USA 2003, 100:4802–4806
6. Harada M, Qin Y, Takano H, Minamino T, Zou Y, Toko H, Ohtsuka M, Matsuura K, Sano M, Nishi J, Iwanaga K, Akazawa H, Kunieda T, Zhu W, Hasegawa H, Kunisada K, Nagai T, Nakaya H, Yamauchi-Takihara K, Komuro I: G-CSF prevents cardiac remodeling after myocardial infarction by activating the Jak-Stat pathway in cardiomyocytes. Nat Med 2005, 11:305–311
7. Orlic D, Kajstura J, Chimenti S, Limana F, Jakoniuk I, Quaini F, Nadal-Ginard B, Bodine DM, Leri A, Anversa P: Mobilized bone marrow cells repair the infarcted heart, improving function and survival. Proc Natl Acad Sci USA 2001, 98:10344–10349
8. Miki T, Miura T, Nishino Y, Yano T, Sakamoto J, Nakamura Y, Ichikawa Y, Ikeda Y, Kobayashi H, Ura N, Shimamoto K: Granulocyte colony stimulating factor/macrophage colony stimulating factor improves postinfarct ventricular function by suppression of border zone remodelling in rats. Clin Exp Pharmacol Physiol 2004, 31:873–882
9. Ohno R, Miyawaki S, Hatake K, Kuriyama K, Saito K, Kanamaru A, Kobayashi T, Kodera Y, Nishikawa K, Matsuda S, Yamada O, Omoto E, Takeyama H, Tsukuda K, Asou N, Tanimoto M, Shiozaki H, Tomonaga M, Masaoka T, Miura Y, Takaku F, Ohashi Y, Motoyoshi K: Human urinary macrophage colony-stimulating factor reduces the incidence and duration of febrile neutropenia and shortens the period required to finish three courses of intensive consolidation therapy in acute myeloid leukemia: a double-blind controlled study. J Clin Oncol 1997, 15:2954–2965
10. Kawakami Y, Nagai N, Ohama K, Zeki K, Yoshida Y, Kuroda E, Yamashita U: Macrophage-colony stimulating factor inhibits the growth of human ovarian cancer cells in vitro. Eur J Cancer 2000, 36:1991–1997
11. Stanley ER, Berg KL, Einstein DB, Lee PS, Pixley FJ, Wang Y, Yeung YG: Biology and action of colony-stimulating factor-1. Mol Reprod Dev 1997, 46:4–10
12. Giordano FJ, Gerber HP, Williams SP, VanBruggen N, Bunting S, Ruiz-Lozano P, Gu Y, Nath AK, Huang Y, Hickey R, Dalton N, Peterson KL, Ross Jr J, Chien KR, Ferrara N: A cardiac myocyte vascular endothelial growth factor paracrine pathway is required to maintain cardiac function. Proc Natl Acad Sci USA 2001, 98:5780–5785
13. Maharaj AS, Saint-Geniez M, Maldonado AE, D'Amore PA: Vascular endothelial growth factor localization in the adult. Am J Pathol 2006, 168:639–648
14. Okazaki T, Ebihara S, Takahashi H, Asada M, Kanda A, Sasaki H: Macrophage colony-stimulating factor induces vascular endothelial growth factor production in skeletal muscle and promotes tumor angiogenesis. J Immunol 2005, 174:7531–7538
15. Kalka C, Masuda H, Takahashi T, Gordon R, Tepper O, Gravereaux E, Pieczek A, Iwaguro H, Hayashi SI, Isner JM, Asahara T: Vascular endothelial growth factor$_{165}$ gene transfer augments circulating endothelial progenitor cells in human subjects. Circ Res 2000, 86:1198–1202
16. Kallies A, Rosenbauer F, Scheller M, Knobeloch KP, Horak I: Accumulation of c-Cbl and rapid termination of colony-stimulating factor 1 receptor signaling in interferon consensus sequence bind-

ing protein-deficient bone marrow-derived macrophages. Blood 2002, 99:3213–3219
17. Novak U, Harpur AG, Paradiso L, Kanagasundaram V, Jaworowski A, Wilks AF, Hamilton JA: Colony-stimulating factor 1-induced STAT1 and STAT3 activation is accompanied by phosphorylation of Tyk2 in macrophages and Tyk2 and JAK1 in fibroblasts. Blood 1995, 86:2948–2956
18. Kelley TW, Graham MM, Doseff AI, Pomerantz RW, Lau SM, Ostrowski MC, Franke TF, Marsh CB: Macrophage colony-stimulating factor promotes cell survival through Akt/protein kinase B. J Biol Chem 1999, 274:26393–26398
19. Ménard C, Pupier S, Mornet D, Kitzmann M, Nargeot J, Lory P: Modulation of L-type calcium channel expression during retinoic acid-induced differentiation of H9C2 cardiac cells. J Biol Chem 1999, 274:29063–29070
20. van den Eijnde SM, van den Hoff MJ, Reutelingsperger CP, van Heerde WL, Henfling ME, Vermeij-Keers C, Schutte B, Borgers M, Ramaekers FC: Transient expression of phosphatidylserine at cell-cell contact areas is required for myotube formation. J Cell Sci 2001, 114:3631–3642
21. Kang YJ, Zhou ZX, Wang GW, Buridi A, Klein JB: Suppression by metallothionein of doxorubicin-induced cardiomyocyte apoptosis through inhibition of p38 mitogen-activated protein kinases. J Biol Chem 2000, 275:13690–13698
22. Okazaki T, Sakon S, Sasazuki T, Sakurai H, Doi T, Yagita H, Okumura K, Nakano H: Phosphorylation of serine 276 is essential for p65 NF-κB subunit-dependent cellular responses. Biochem Biophys Res Commun 2003, 300:807–812
23. Seno H, Oshima M, Ishikawa TO, Oshima H, Takaku K, Chiba T, Narumiya S, Taketo MM: Cyclooxygenase 2- and prostaglandin E_2 receptor EP_2-dependent angiogenesis in $Apc^{\Delta 716}$ mouse intestinal polyps. Cancer Res 2002, 62:506–511
24. Bildfell RJ, Valentine BA, Whitney KM: Cutaneous vasoproliferative lesions in goats. Vet Pathol 2002, 39:273–277
25. Ebihara S, Guibinga GH, Gilbert R, Nalbantoglu J, Massie B, Karpati G, Petrof BJ: Differential effects of dystrophin and utrophin gene transfer in immunocompetent muscular dystrophy (mdx) mice. Physiol Genomics 2000, 3:133–144
26. Sakon S, Xue X, Takekawa M, Sasazuki T, Okazaki T, Kojima Y, Piao JH, Yagita H, Okumura K, Doi T, Nakano H: NF-κB inhibits TNF-induced accumulation of ROS that mediate prolonged MAPK activation and necrotic cell death. EMBO J 2003, 22:3898–3909
27. Wang Q, Yambe T, Shiraishi Y, Duan X, Nitta S, Tabayashi K, Umezu M: An artificial myocardium assist system: electrohydraulic ventricular actuation improves myocardial tissue perfusion in goats. Artif Organs 2004, 28:853–857
28. Kim WG, Cho SR, Sung SH, Park HJ: A chronic heart failure model by coronary artery ligation in the goat. Int J Artif Organs 2003, 26:929–934
29. Eubank TD, Galloway M, Montague CM, Waldman WJ, Marsh CB: M-CSF induces vascular endothelial growth factor production and angiogenic activity from human monocytes. J Immunol 2003, 171:2637–2643
30. Ide H, Seligson DB, Memarzadeh S, Xin L, Horvath S, Dubey P, Flick MB, Kacinski BM, Palotie A, Witte ON: Expression of colony-stimulating factor 1 receptor during prostate development and prostate cancer progression. Proc Natl Acad Sci USA 2002, 99:14404–14409
31. Baines CP, Molkentin JD: STRESS signaling pathways that modulate cardiac myocyte apoptosis. J Mol Cell Cardiol 2005, 38:47–62
32. Valks DM, Cook SA, Pham FH, Morrison PR, Clerk A, Sugden PH: Phenylephrine promotes phosphorylation of Bad in cardiac myocytes through the extracellular signal-regulated kinases 1/2 and protein kinase A. J Mol Cell Cardiol 2002, 34:749–763
33. Matsui T, Rosenzweig A: Convergent signal transduction pathways controlling cardiomyocyte survival and function: the role of PI 3-kinase and Akt. J Mol Cell Cardiol 2005, 38:63–71
34. Arsic N, Zacchigna S, Zentilin L, Ramirez-Correa G, Pattarini L, Salvi A, Sinagra G, Giacca M: Vascular endothelial growth factor stimulates skeletal muscle regeneration in vivo. Mol Ther 2004, 10:844–854
35. Yano T, Miura T, Whittaker P, Miki T, Sakamoto J, Nakamura Y, Ichikawa Y, Ikeda Y, Kobayashi H, Ohori K, Shimamoto K: Macrophage colony-stimulating factor treatment after myocardial infarction attenuates left ventricular dysfunction by accelerating infarct repair. J Am Coll Cardiol 2006, 47:626–634
36. Rutanen J, Rissanen TT, Markkanen JE, Gruchala M, Silvennoinen P, Kivela A, Hedman A, Hedman M, Heikura T, Orden MR, Stacker SA, Achen MG, Hartikainen J, Yla-Herttuala S: Adenoviral catheter-mediated intramyocardial gene transfer using the mature form of vascular endothelial growth factor-D induces transmural angiogenesis in porcine heart. Circulation 2004, 109:1029–1035
37. Azuma J, Taniyama Y, Takeya Y, Iekushi K, Aoki M, Dosaka N, Matsumoto K, Nakamura T, Ogihara T, Morishita R: Angiogenic and antifibrotic actions of hepatocyte growth factor improve cardiac dysfunction in porcine ischemic cardiomyopathy. Gene Ther 2006, 13:1206–1213
38. Bhatt NY, Kelley TW, Khramtsov VV, Wang Y, Lam GK, Clanton TL, Marsh CB: Macrophage-colony-stimulating factor-induced activation of extracellular-regulated kinase involves phosphatidylinositol 3-kinase and reactive oxygen species in human monocytes. J Immunol 2002, 169:6427–6434
39. Gobert Gosse S, Bourgin C, Liu WQ, Garbay C, Mouchiroud G: M-CSF stimulated differentiation requires persistent MEK activity and MAPK phosphorylation independent of Grb2-Sos association and phosphatidylinositol 3-kinase activity. Cell Signal 2005, 17:1352–1362
40. Lipovetsky G, Fenoglio JJ, Gieger M, Srinivasan MR, Dobelle WH: Coronary artery anatomy of the goat. Artif Organs 1983, 7:238–245

Available online at www.sciencedirect.com
ScienceDirect
Medical Engineering & Physics 29 (2007) 840–844
Medical Engineering & Physics
www.elsevier.com/locate/medengphy

Passive mechanical properties of large intestine under *in vivo* and *in vitro* compression

Masaru Higa[a,*], Yun Luo[a], Takeshi Okuyama[b], Toshiyuki Takagi[b], Yasuyuki Shiraishi[c], Tomoyuki Yambe[c]

[a] *Biomedical Engineering Research Organization, Tohoku University, Sendai, Japan*
[b] *Institute of Fluid Science, Tohoku University, Sendai, Japan*
[c] *Institute of Developing, Aging and Cancer, Tohoku University, Sendai, Japan*

Received 17 February 2006; received in revised form 7 September 2006; accepted 12 September 2006

Abstract

This paper presents experimental data obtained from both *in vivo* and *in vitro* compression of the large intestine of goat. *In vivo* experimental data were obtained from compression tests on the large intestine of an anesthetized goat using force–displacement acquisition equipment. *In vitro* experimental data were also obtained from tissue excised after the *in vivo* experiments, and two types of data were then compared. The results demonstrated that the stress values had a strong dependence on the compressive rate in the *in vivo* experiments, although such effect was not distinct in the *in vitro* experiments. Additionally, at a lower compression rate, the intestinal tissues were found to be stiffer in the *in vitro* experiments than in the *in vivo* ones. This paper is a preliminary report on the mechanical properties of the large intestine based on *in vivo* and *in vitro* experimental data.

Keywords: Large intestine; Mechanical property; *In vivo* test; Soft tissues

1. Introduction

Continued developments of implantable artificial internal organs and computer-aided surgery, as well as of virtual reality techniques, will require closer examination of the mechanical properties of soft tissues and, ultimately, the construction of appropriate mathematical models. As a completely implantable artificial organ, the authors are now developing an artificial anal sphincter using shape memory alloys with a structure that sandwiches the large intestine. This device is being developed as a minimally invasive prosthesis with a simple structure to solve the problem of severe fecal incontinence. Details have been presented in previous reports [1,2]. Measuring the mechanical properties of the large intestine will be very important for the development of this device. In order to predict the tissue response by finite element (FE) analysis, the intrinsic stress–strain behavior of the tissue must be determined. Many researchers have examined the mechanical properties of soft tissues and some reports have been published regarding the large intestine [3–7]. However, most reports about the large intestine have been based on tensile examinations, in which samples that had been surgically excised from animals or humans were pulled on a tensiometer, the tensile test being a well-used technology in material characterization. It means *in vitro* test. To date, very little quantitative information has been available on the biomechanical properties of soft tissue *in vivo* [8,9] and no studies have been undertaken to examine the mechanical properties of the large intestine *in vivo*. The biomechanical properties of soft tissues may show different values depending on whether they are measured *in vivo* or *in vitro* because, the viability and mechanical properties of the samples are affected when the neurovascular supply serving the large intestine is impaired [10].

The purpose of this study is to measure the stress–strain relations of the large intestine by both *in vivo* and *in vitro* compression and to compare the resulting two types of data.

* Corresponding author. Tel.: +81 79 267 4839; fax: +81 79 267 4839.
E-mail address: higa@eng.u-hyogo.ac.jp (M. Higa).

1350-4533/$ – see front matter © 2006 IPEM. Published by Elsevier Ltd. All rights reserved.
doi:10.1016/j.medengphy.2006.09.003

The compression method was chosen to obtain comprehensive information about the passive response of soft tissue to contact with implantable artificial internal organs. These data are relevant to predict the stress distribution in the tissue when the force value from prosthesis or other surgical instruments was distinct.

2. Materials and methods

2.1. Specimen preparation

An adult nanny-Saanen goat was used in this experiment because the diameter of the bowel in a goat is close to that of the human bowel. After intramuscular administration of atropine sulfate, anesthesia was induced via an endotracheal tube and maintained with 2.5% halothane. Anesthesia was maintained throughout the experiment. The respiration rate was fixed at 15 min^{-1} by a respirator and the heart rate was approximately $126 \pm 10\,min^{-1}$. The weight of the goat was approximately 50 kg. Before celiotomy, pancuronium bromide was injected intravenously to block contractile activity in the gastrointestinal tract. After achievement of smooth muscle relaxation, a part of the descending colon was bilaterally exposed by celiotomy. The proximal part from the arteria mesenterica caudalis was used as an experimental sample. A supporting plate required for the compression experiment was inserted into the intestinal lumen through a small incision in the intestinal wall. The residual contents in the lumen were gently cleared using physiological saline. Special care was taken to maintain the viability of the tissue during the *in vivo* experiments by preserving the neurovascular supply serving the large intestine. Compression experiments were performed in one animal in which the position of applied compression was changed in each test. After the *in vivo* procedure, a portion of the tissue was excised for use in the *in vitro* experiments. The position of compression differed in all the examinations compression because compression damages the tissue. The tissue was immediately immersed in iced physiological saline and the *in vitro* experiments were performed within 6 h after the excision. We warmed the tissue up to 37 °C again before *in vitro* compression.

2.2. Experimental setup

Uniaxial compression of the large intestine was performed using a testing device as shown in Fig. 1. The intestinal wall was compressed between the supporting plate and a cylindrical, movable platen (2 mm in diameter) fixed to a load cell (UT-500GR, rated capacity = 4.9 N, Minebea Co., Ltd.). The load cell was fixed on the mover of a one-axis stage controller (QT-CD1, Chuo Precision Industrial Co., Ltd.). The supporting plate, inserted into the intestinal lumen, was fixed to the stator of the stage controller. The compression loads and displacements were simultaneously recorded and the stage movement was controlled by a personal computer connected to the stage controller. The thicknesses of the tissue sample were measured before each experiment by a laser displacement meter (LB-60, Keyence, Co., Ltd.) attached to the stage controller. Both the supporting plate and the movable cylindrical platen were made of acrylic resin.

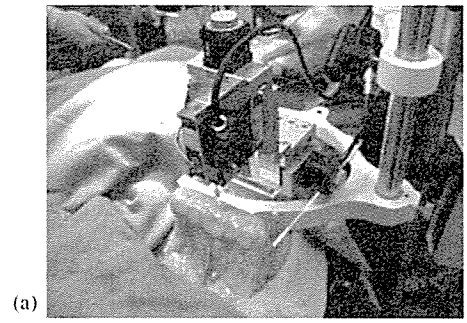

(a)

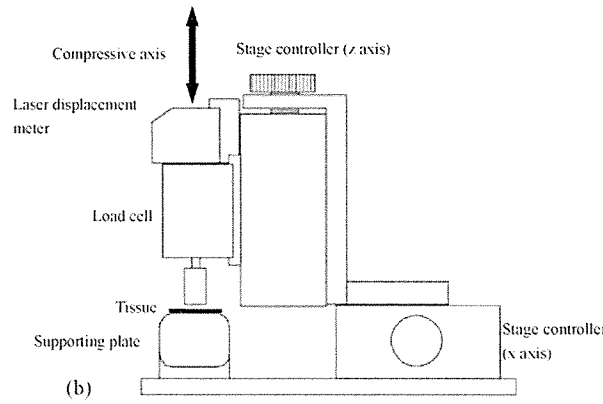

Fig. 1. ***In vivo*** **experimental configuration: an overview of testing (a), and a schematic illustration of the set-up (b). A supporting plate was inserted in the intestinal lumen from the incision beside the compression position oriented to the longitudinal direction.**

2.3. Experimental protocol

The compressive rate (V_0) was set at 0.02 mm/s, 0.5 mm/s, or 5 mm/s. The data sampling frequency was set at 100 Hz. The movement of the movable platen began about 2 mm above the supporting plate, a sufficient distance compared to the tissue thickness, and stopped at 0.2 mm above the supporting plate. Measurements were performed at the different rates, three times each at different positions in one tissue sample. Each three compressions result was averaged using commercially available scientific graphing and analysis software (ORIGIN (R) 6.1, OriginLab, Co., MA). No preconditioning test was done. Throughout the entire experiment, the large intestine was moistened by a jet of physiological saline. At the end of the experiment, no signs of dehydration were observed. Both the *in vivo* and *in vitro* experiments were performed using the same protocol described above.

3. Experimental results

The data obtained from the experiments were forces and displacements. To enable a comprehensive comparison, the forces and displacements were converted to stress and strain taking the compression platen area (2 mm in diameter circle) and the thickness of the samples into account, respectively. In this study, stresses in radial direction of the colon and nominal strains were calculated. Fig. 2 shows the stress–strain curves of tissues subjected to *in vivo* compression tests. In Fig. 2(a)–(c) represent the data obtained at different compressive rates, namely 0.02 mm/s, 0.5 mm/s, and 5 mm/s, respectively. In each figure, the three curves represent the experimental iteration. The differences in the end values of strain between the curves are due to slight differences in the tissue thickness at the corresponding compression position.

Fig. 3 shows the stress–strain curves obtained from the *in vitro* compression. The experimental conditions were the same as those used in the *in vivo* tests. In the case of $V_0 = 0.02$ mm/s, one result was excluded because of experimental error.

The average tissue thickness was 1.11 (±0.25) mm. Each strain rate was 0.018 s^{-1} (0.02 mm/s), 0.45 s^{-1} (0.5 mm/s) and 4.50 s^{-1} (5 mm/s), respectively. These strain values were calculated from average tissue thickness. Real strain values of each sample depended on each tissue thickness (not shown in this manuscript).

A comparison of the stress–strain curves between the *in vivo* and *in vitro* experiments is shown in Fig. 4. Each curve represents the mean value of results obtained under the same condition. It was found that, while the *in vitro* results were less dependent on the compression rates, the *in vivo* results were strongly dependent on the compression rates. There was a significant difference between the results obtained at the lower rates (0.02 mm/s and 0.5 mm/s), and those at the higher rate (5 mm/s) in the *in vivo* tests. Absolute stress values at $\varepsilon = 0.7$ for instance, were 14.72 kPa (0.02 mm/s, vivo), 25.45 kPa (0.5 mm/s, vivo), 120.46 kPa (5 mm/s, vivo), 136.23 kPa (0.02 mm/s, vitro), 133.97 kPa (0.5 mm/s, vitro) and 204.76 kPa (5 mm/s, vitro), respectively.

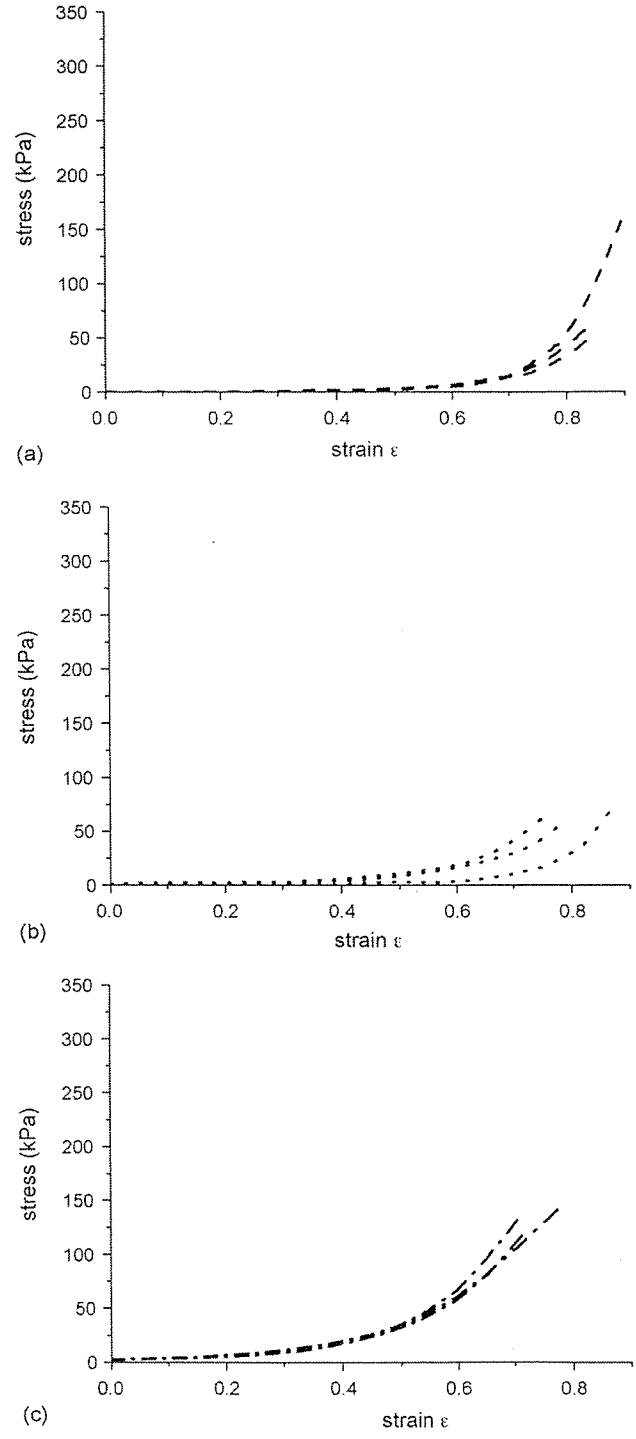

Fig. 2. Stress–strain curves under *in vivo* compression. $V_0 = 0.02$ mm/s (a), $V_0 = 0.5$ mm/s (b) and $V_0 = 5$ mm/s (c).

4. Discussion

One difficulty in such measurement is to determine the starting point of the stress–strain curves because the force between the platen and the tissue in the case of soft tissue appears negligibly small at the beginning of contact. Misreading of the starting point may cause the omission of a significant amount of information about the tissues. In this work, the starting point was determined using the thickness of the tissue at the targeted point, which was measured in advance by a laser displacement meter.

The apparent limitation of this study is that experiments were conducted on one animal though compressions were repeated three times. We finally want mechanical properties of human organs. More animal experiments give us average mechanical properties of animal organs only. To know mechanical properties of human organs in future, this study was conducted using experimental animal as a first step. More sacrifice of experimental animals will not be meaningful in the next step. As mechanical parameters of human organs, Carter et al. reported the measurements from human intra-

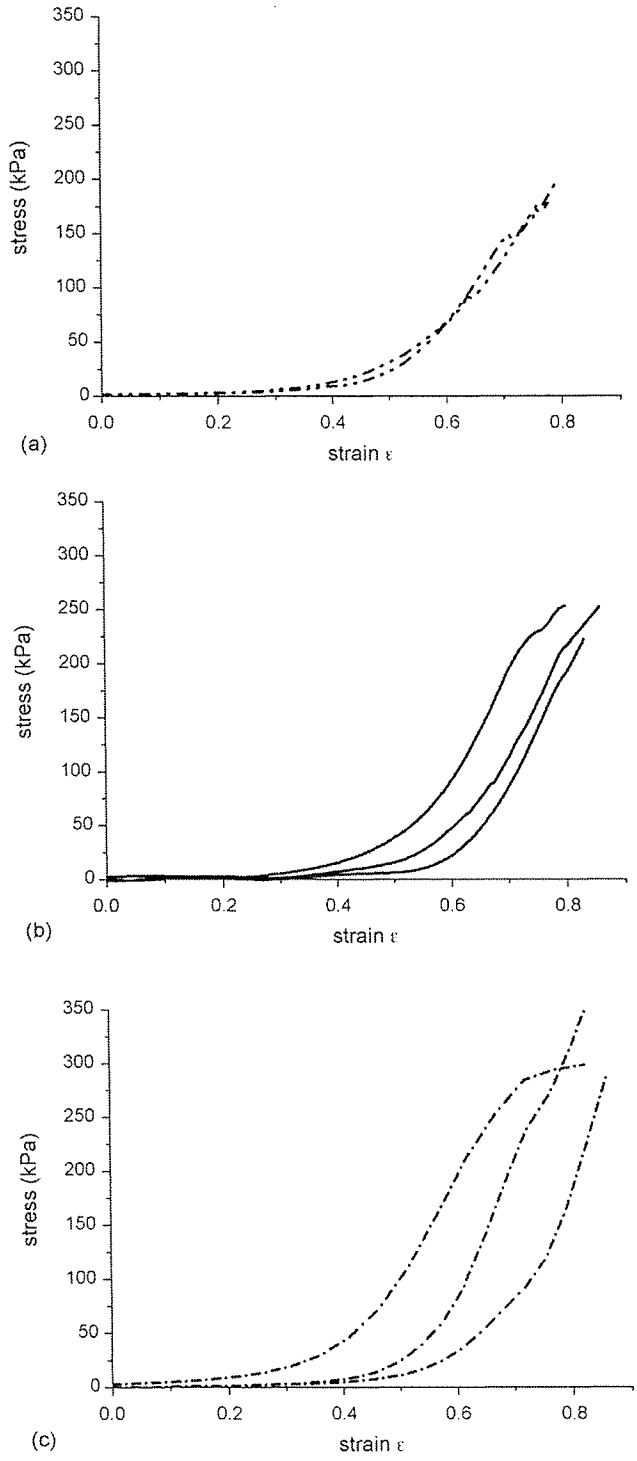

Fig. 3. Stress–strain curves under *in vitro* compression. $V_0 = 0.02$ mm/s (a), $V_0 = 0.5$ mm/s (b) and $V_0 = 5$ mm/s (c).

abdominal organs *in vivo*. It was the first example of such data had being obtained from living human subjects [9]. They treated, however, only solid organs. The large intestine that we wanted to measure is hollow organ. Histologically, hollow organs cannot be treated as isotropic and homogeneous. So the data presented in this paper has to be considered that the tissue response, the stress–strain behavior when load was applied to radial direction. This data is meaningful because tissue is loaded most frequently in this way when artificial anal sphincter is implanted. The stress–strain tissue response with artificial anal sphincter is required for us to develop this prosthesis. Off course, to reveal the real stress distribution considering anisotropy and heterogeneity is meaningful as a future study.

Concerning the differences between the *in vivo* and *in vitro* results of biological tissue, Miller et al. compared results of *in vivo* compression of swine brain with *in vitro* experimental results [11,12]. They reported that the force predicted by the FE model based on *in vitro* compression was about 31% lower than that obtained by *in vivo* measurement. On the other hand, the present results showed that the tissue was stiffer *in vitro* than *in vivo*. The results had contrariety. There is fairly general agreement that mechanical properties of soft tissue show different values depending on whether the tissue is measured *in vivo* or *in vitro*. The difference between their results and the present results is not surprising since changes may occur when tissue is dissected from a living body, and such changes may affect the intrinsic mechanical parameters of the tissue. Thus, it is appropriate to consider that differences in the experimental conditions, the tissue examined (brain or large intestines), the species (pig or goat), the compression rates, the experimental setup and the protocols could affect the results. The difference of tissue region (brain or large intestine) particularly may affect this contrariety. The difference of anatomical structure of each organ may affect the mechanical properties. This study was a first report about *in vivo* tests of large intestine.

In Fig. 4, it can be seen that in the *in vivo* tests the tissue have lower stiffness than *in vitro* tests. An acceptable supposition is that living tissues have viscoelastic properties with shorter relaxation time than *in vitro* tissue. It is also noteworthy that the results strongly depended on the starting

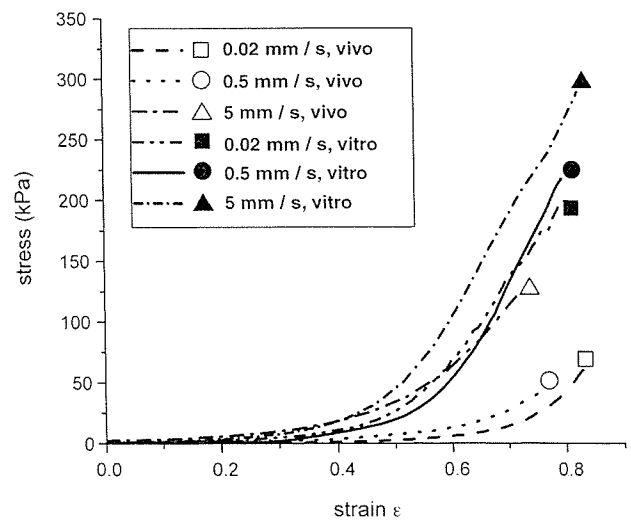

Fig. 4. Stress–strain curves of all compressive rates. Each graph represents the mean values of each compressive rate both *in vivo* and *in vitro*.

point (or point of contact) of stress–strain data. That is, without an accurate measurement of the point of contact in the compression direction, it would be difficult to obtain reliable information for comparison of results obtained at different compression rates. As described above, the accurate measurement of tissue thickness with a laser displacement meter enabled us to avoid this difficulty.

5. Conclusions

In this paper, both the *in vivo* and *in vitro* compression results of goat large intestine were presented. While the *in vitro* results showed less dependence on the compression rates, the *in vivo* results were strongly dependent on the compression rates. There was a significant difference between the results at the lower and higher rates in the *in vivo* tests. That is, at the lower rates, the tissue appeared softer.

In conclusion, comparison of the *in vivo* and *in vitro* compression results showed the risk of using only *in vitro* data in numerical simulations or modeling of tissue. *In vivo* data must be taken into account in studies of the passive mechanical response of the large intestine to contact with implantable artificial organs such as an artificial sphincter. In order to simulate the stress–strain relations of the human large intestine *in vivo*, further studies are required to clarify what happens histologically or morphologically when tissue is excised from a living body and how this affects the tissue stiffness.

References

[1] Luo Y, Takagi T, Okuyama T, Amae S, Wada M, Nishi K, et al. Functional evaluation of an artificial anal sphincter using shape memory alloys. ASAIO J 2004;50(4):338–43.
[2] Luo Y, Higa M, Amae S, Yambe T, Okuyama T, Takagi T, et al. The possibility of muscle tissue reconstruction using shape memory alloys. Organogenesis 2005;2(1):2–5.
[3] Egorov VI, Schastlivtsev IV, Prut EV, Baranov AO, Torso RA. Mechanical properties of the human gastrointestinal tract. J Biomech 2002;35:1417–25.
[4] Gao C, Gregersen H. Biomechanical and morphological properties in rat large intestine. J Biomech 2000;33:1089–97.
[5] Watters DA, Smith AN, Eastwood MA, Anderson KC, Elton RA. Mechanical properties of the rat colon: the effect of age, sex and different conditions of storage. Q J Exp Physiol 1985;70(1):151–62.
[6] Yamada H. Strength of biological materials. 2nd ed. Baltimore: Williams and Watkins; 1972.
[7] Qiao Y, Pan E, Chakravarthula SS, Han F. Measurement of mechanical properties of rectal wall. J Mater Sci: Mater Med 2005;16:183–8.
[8] Bosboom EMH, Hesselink MKC, Oomens CWJ, Bouten CVC, Drost MR, Baaijens FPT. Passive transverse mechanical properties of skeletal muscle under *in vivo* compression. J Biomech 2001;34:1365–8.
[9] Carter FJ, Frank TG, Davis PJ, McLean D, Cuschieri A. Measurements and modeling of the compliance of human and porcine organs. Med Image Anal 2001;5:231–6.
[10] Han L, Alison N, Burcher M. A novel ultrasound indentation system for measuring biomechanical properties of *in vivo* soft tissue. Ultrasound Med Biol 2003;29(6):813–23.
[11] Miller K. Constitutive model of brain tissue suitable for finite element analysis of surgical procedure. J Biomech 1999;32:531–7.
[12] Miller K, Chinzei K, Orssengo G, Bednarz P. Mechanical properties of brain tissue *in vivo*: experiment and computer simulation. J Biomech 2000;33:1369–76.

Tohoku J. Exp. Med., 2006, **209**, 15-21

Impact of Type A Behavior on Brachial-Ankle Pulse Wave Velocity in Japanese

HONGJIAN LIU, YOSHIFUMI SAIJO, XIUMIN ZHANG,[1] YASUYUKI SHIRAISHI, YUN LUO,[2] MITSUYA MARUYAMA,[3] MASARU HIGA,[2] KAZUMITSU SEKINE and TOMOYUKI YAMBE

Department of Medical Engineering and Cardiology, Institute of Development, Aging and Cancer, Tohoku University, Sendai, Japan,
[1] Department of Medicine and Science in Sports and Exercise, Tohoku University Graduate School of Medicine, Sendai, Japan,
[2] Biomedical Engineering Research Organization, Tohoku University, Sendai, Japan, and
[3] Division of Medical Engineering and Clinical Investigation, Institute of Development, Aging and Cancer, Tohoku University, Sendai, Japan

LIU, H., SAIJO, Y., ZHANG, X., SHIRAISHI, Y., LUO, Y., MARUYAMA, M., HIGA, M., SEKINE, K. and YAMBE, T. *Impact of Type A Behavior on Brachial-Ankle Pulse Wave Velocity in Japanese*. Tohoku J. Exp. Med., 2006, **209** (1), 15-21 —— Pulse wave velocity (PWV) is the velocity of a pulse wave traveling a given distance between 2 sites in the arterial system, and is a well-known indicator of arteriosclerosis. Brachial-ankle PWV (baPWV) is a parameter more simple to obtain, compared with the conventional PWV, and is an easy and effective means of evaluating arteriosclerosis. BaPWV can be obtained by only wrapping the four extremities with blood pressure cuffs, and it can be easily used to screen a large number of subjects. Type A behavior has been confirmed as an independent risk factor for the development of coronary heart disease. To examine the relationship between Type A behavior and arteriosclerosis, 307 normal Japanese subjects were classified into either a Type A group (n = 90) or a non-Type A group (n = 217) by using Maeda's Type A Scale. BaPWV was evaluated using a PWV diagnosis device. The baPWV in the Type A group was significantly higher than that obtained in the non-Type A group. The baPWV showed a positive correlation with age both in the Type A group and in the non-Type A group; however, the straight-line regression slope of baPWV versus age in the Type A group was significantly larger than that in the non-Type A group. Therefore, our results suggest that arteriosclerosis might be promoted earlier in subjects expressing the Type A behavior pattern. Type A behavior pattern is confirmed as a risk factor for arteriosclerosis, and may increase the risk of the cardiovascular disease related to arteriosclerosis. ——— Type A behavior; Brachial-ankle pulse wave velocity; arteriosclerosis

Received December 14, 2005; revision accepted for publication March 6, 2006.
Correspondence: Hongjian Liu, Ph.D., Department of Medical Engineering and Cardiology, Institute of Development, Aging and Cancer, Tohoku University, 4-1 Seiryomachi, Aoba-ku, Sendai 980-8575, Japan.
e-mail: hongjianliu63@yahoo.co.jp

Type A behavior was first described by Friedman and Rosenman in the late 1950s, and it has since drawn considerable attention as a possible coronary risk factor. This behavior pattern includes impatience, aggressiveness, a sense of time urgency, an intense achievement drive, and a desire for recognition and advancement. In the Western Collaborative Group Study, the Type A behavior pattern was shown to be predictive of the incidence of coronary heart disease independently of the traditional risk factors such as smoking, hyperlipidemia, and hypertension (Buller et al. 1998; Yoshimasu 2001). Type A behavior may enhance the rate of development of coronary arteriosclerosis, and the presence and severity of coronary arteriosclerosis as determined by angiography have been investigated in relation to the presence and severity of Type A behavior (Sparagon et al. 2001). Type A behavior assessed by a questionnaire modified to Japanese characteristics and job strain has been linked to angiographically determined coronary arteriosclerosis (Yoshimasu et al. 2000; Gallacher et al. 2003).

Pulse wave velocity (PWV) is a well known indicator of arteriosclerosis. Many reports have described the relationship between PWV and the development of arteriosclerotic disease. Recent studies have demonstrated that PWV is not only a risk marker of cardiovascular disease, but is also a prognostic predictor (Altun et al. 2004; Fujiwara et al. 2004; Tomiyama et al. 2004, 2005; Woodside et al. 2004).

PWV is the velocity of a pulse wave traveling a given distance between 2 sites in the arterial system. Recently, a new, simple device to measure brachial-ankle pulse wave velocity (baPWV) has been developed using pressure cuffs wrapped around the brachium and ankle. BaPWV has potential as a new marker of cardiovascular risk over conventional markers, as it is easy to obtain and serves as an indicator of either arteriosclerotic cardiovascular risk or severity of arteriosclerotic vascular damage. Thus it can be useful in screening the general population (Yamashina et al. 2003; Yokoyama et al. 2003; Ogawa et al. 2005).

Therefore, we hypothesized that if Type A behavior could be a risk factor of arteriosclerosis, subjects expressing the Type A behavior pattern might show a higher baPWV. The aim of this study was to compare differences of baPWV between subjects showing Type A behavior and those not showing Type A behavior.

Materials and Methods

Subjects

Three hundreds and seven normal Japanese subjects participated in this study. The data were collected at Tohoku University, Sendai, Japan. The exclusion criteria were the following: hypertension (defined as systolic blood pressure [SBP] ≧ 140 mmHg, diastolic blood pressure [DBP] ≧ 90 mmHg, or drug treatment for hypertension), endocrine disease, significant renal or hepatic disease, coronary artery disease, arrhythmias, cerebrovascular disease, or use of medication for diabetes mellitus or hyperlipidemia. Written informed consent was obtained from all participants, and the study protocol was approved by the Ethics Committee of Tohoku University, Graduate School of Medicine and School of Medicine, Japan.

Measurement of the Type A behavior pattern

Type A behavior was assessed by an abbreviated set of 12 questions developed by Maeda (1991). This assessment is considered to be very practical for epidemiological investigations because of its convenience. Each question is listed in Table 1. The subjects were asked to answer all of the questions. Each question allowed three responses. Two, 1, and 0 points were assigned, respectively, to responses of "always", "occasionally", and "hardly" for questionnaire items 1, 2, 3, 4, 7, 8, 10, 11, and 12, and the points were doubled for questionnaire items 5, 6, and 9. A total score of 17 or greater was defined as Type A.

Measurement of baPWV

The subjects were examined while resting in the supine position. After at least a 5-minute bed rest, baPWV was recorded using an automated device (VaSeraVS-1000, Fukuda Denshi, Tokyo) (Liu et al. 2005; Watanabe et al. 2005). This device simultaneously records baPWV, blood pressure (BP), electrocardiogram, and heart sounds. Electrocardiogram electrodes were placed on both wrists, and a heart sound microphone was placed on the left sternal border. Cuffs to measure baPWV were wrapped around both upper arms and ankles, and connected to a plethysmographic sensor that